

Investigating weathering signatures in terrestrial muds: Can climatic signatures be separated from provenance?

Cansu Demirel-Floyd^{1,†}, Gerilyn S. Soreghan¹, Nina D.S. Webb², Autumn Roche¹, Young Ji Joo³, Brenda Hall⁴, Joseph S. Levy⁵, Andrew S. Elwood Madden¹, and Megan E. Elwood Madden¹

¹School of Geosciences, University of Oklahoma, Norman, Oklahoma 73019, USA

ABSTRACT

Siliciclastic muds (clay- and silt-sized sediment) concentrate physical and chemical weathering products. However, both rock composition and climate can affect the mineralogy and geochemistry of these sediments. We quantitatively assessed the influence of provenance and climate on muds collected from end-member climates to test, which, if any, of these potential weathering signatures are indicative of climate in finegrained, fluvial sediments. Granulometry, mineralogy, and geochemistry of the studied muds indicated that provenance and mineral sorting hinder interpretation of (paleo)climate signals. These issues also affect chemical index of alteration (CIA) values, as well as mafic-felsic-weathering (MFW), Al₂O₃-(CaO* + Na₂O)-K₂O (A-CN-K), and Al₂O₃-(CaO* + Na₂O + K₂O)-(FeOT + MgO) (A-CNK-FM) ternary plots, decreasing their utility as paleoclimate proxies. CaO content is heavily weighted within the calculations, resulting in even felsic-sourced sediment commonly plotting as mafic owing to the relative enrichment in CaO from preferential sorting of Ca-rich minerals into the mudsized fraction during transport. These results cast doubt on the indiscriminate use of CIA values and ternary plots for interpreting chemical weathering and paleoclimate within muds, particularly from glacial systems.

Most notably, the positive correlations between CIA and climatic parameters (mean annual temperature and mean annual pre-

Gerilyn S. Soreghan https://orcid.org/0000 -0001-6925-5675 †cansudemirel@gmail.com cipitation) diminished when sediments that had formed in nonglacial settings were filtered out from the data sets. This implies that CIA may only be applicable when used in nonglacial systems in which the composition of the primary source material is well constrained—such as soil/paleosol profiles. Within this end-member climate data set, CIA was only useful in discriminating hothumid climates.

INTRODUCTION

Chemical weathering has been a fundamental component of Earth surface processes throughout geologic time, producing chemical, physical, and mineralogical signatures within siliciclastic sediments (White et al., 1996). Chemical weathering of silicates is controlled by lithology (composition and texture), climate (temperature and precipitation), biological activity (macroscale and microscale), chemistry of weathering solutes (acidic, neutral, or basic; saline or fresh), and the reactive surface area of fine-grained sediments (White and Peterson, 1990; White and Blum, 1995; White et al., 1996; White and Brantley, 2003; White and Buss, 2014). Weathering products, such as clay minerals and Feoxides, are concentrated within the mud-sized (<63 μm) sediment fraction due to their small grain sizes (Nesbitt and Young, 1982). Climate regime and duration of weathering are thought to largely control the type and amount of secondary weathering products. For example, the highest intensity of chemical alteration and most abundant secondary mineral products such as kaolinite and Fe-oxides would be expected to occur in hot and humid (tropical) settings. Likewise, negligible chemical weathering and less-aluminous clays (illite, smectite, and chlorite) are associated

with dry, high-latitude regions, including glacial systems (Biscaye, 1965; Barshad, 1966; Nesbitt and Young, 1982; Velbel, 1993; White et al., 1999; White and Brantley, 2003). However, these weathering product—climate relationships are not always reflected in geochemical weathering assessments. For example, high values of the chemical index of alteration (CIA; Nesbitt and Young, 1982) have been reported within some glacial regions (e.g., Marra et al., 2017) comparable to those of tropical settings (i.e., Joo et al., 2018a; Webb et al., 2022).

Evidence of chemical weathering has long been utilized for paleoclimate interpretations based on weathering indices calculated from major-oxide compositions of sediment developed on various basement rocks (i.e., CIA; Nesbitt and Young, 1982; Soreghan and Soreghan, 2007; Goldberg and Humayun, 2010; Xiao et al., 2010; Li and Yang, 2010; Bahlburg and Dobrzinski, 2011; Yang et al., 2016; Ren et al., 2019; Wang et al., 2020; Deng et al., 2022). Relationships between climate parameters such as mean annual temperature (MAT) and mean annual precipitation (MAP) and CIA show moderate to strong correlations when applied to tropical and temperate regions where weathering trends can be easily observed within well-developed soil profiles (i.e., Nesbitt and Young, 1989; Rasmussen et al., 2011; Yang et al., 2016; Joo et al., 2018a). However, the application of weathering indices, including CIA, in glacial regions produces values that do not follow the same trends as those observed in ice-free systems (Joo et al., 2018a; Deng et al., 2022).

In addition, the physical sorting of grains during sediment transport can also affect chemical weathering signatures by concentrating mechanically weaker minerals (commonly mafic phases) in the finer size fractions (Nesbitt

GSA Bulletin; May/June 2024; v. 136; no. 5/6; p. 2237–2255; https://doi.org/10.1130/B36888.1. Published online 28 September 2023

²Impossible Sensing, St. Louis, Missouri 63118, USA

³Department of Earth and Environmental Sciences, Pukyong National University, Busan 48513, Republic of Korea

⁴School of Earth and Climate Sciences and Climate Change Institute, University of Maine, Orono, Maine 04469, USA

⁵Department of Earth & Environmental Sciences, Colgate University, Hamilton, New York 13346, USA

et al., 1996; von Eynatten et al., 2012). Sorting may lead to underestimated values of weathering indices within fine-grained sediments and regolith, due to the relative enrichment of CaO in the fine-grained sediment fraction (i.e., Nesbitt et al., 1996; Siebach et al., 2017). Despite these complications, CIA and other weathering indices have been widely applied to fine-grained sediments from a large variety of depositional environments, including glacial drifts and fluvial systems on Earth and Mars, where welldeveloped weathering profiles are not available (i.e., Soreghan and Soreghan, 2007; Xiao et al., 2010; Bahlburg and Dobrzinski, 2011; Yang et al., 2016; Marra et al., 2017; Siebach et al., 2017; Hurowitz et al., 2017; Ren et al., 2019; Wang et al., 2020). Since CIA and other weathering indices were developed primarily to interpret weathering intensity in paleosols formed in temperate to tropical settings, it is important to understand and test potential relationships between climate and weathering indices when applied to glacial and fluvial systems, particularly in environments where paleosols are absent or uncommon.

While most previous studies of CIA and other weathering indices have focused primarily on temperate and tropical climate systems (i.e., Nesbitt and Young, 1989; Rasmussen et al., 2011; Yang et al., 2016; Joo et al., 2018a), the effects of extreme end-member climate conditions, including glacial environments, on terrestrial sediment composition, texture, and mineralogy have not been systematically compared. Here, we report the surface area, grain size, mineralogy, and geochemistry of fine-grained glacial and proglacial siliciclastic sediments collected from cold-arid (Antarctic McMurdo Dry Valleys), temperatearid (Peru), and temperate-humid (Norway, Washington, Iceland) glacial systems, as well as fluvial siliciclastic sediments and soils collected from hot-arid (Anza Borrego Desert, California) and hot-humid (Puerto Rico) nonglacial environments to determine if weathering products and chemical weathering indices are controlled by the climate regime of these depositional settings.

We focused on comparison of sediments systematically collected from slack-water regions within fluvial settings traversing similar bedrock types (granitic or granodioritic in all cases except Iceland), which have been treated and analyzed following identical protocols, minimizing user error— and sample treatment—related variations that can occur when reanalyzing compendiums of published data (e.g., Li and Yang, 2010; Deng et al., 2022).

GEOLOGICAL SETTING

We selected drainage basins sited on felsicintermediate bedrock in Antarctica (Stumpf et al., 2012; Marra et al., 2014, 2015, 2017), Norway (Joo et al., 2018b), Peru, Washington State, Puerto Rico (Joo et al., 2018a; Webb et al., 2022), and Southern California (Joo et al., 2016). For these sites, we attempted to keep bedrock composition as similar as possible, but unavoidable variations occur. In addition, we also included samples collected from a basaltic watershed from Iceland to compare the effects of a mafic bedrock source in a glaciated system. We focused primarily on first-cycle sediment, rather than soils, to better control for variable time of soil genesis across field sites, although we include some soil profiles. Summary descriptions for each field area are described below and listed in Table 1, with further details available in the Supplemental Material for this article and within the public data set by Demirel-Floyd (2022) as well as previous papers (Hall et al., 1993, 2000; Levy et al., 2011; Stumpf et al., 2012; Marra et al., 2014, 2015, 2017; Soreghan et al., 2016; Joo et al., 2016, 2018a, 2018b, 2022; Webb et al., 2022), including detailed maps showing specific sampling locations.

¹Supplemental Material. Supplemental materials contain metadata (descriptions, geographic locations) and all analysis results discussed in the text. Please visit https://doi.org/10.1130/GSAB.S.23900184 to access the supplemental material, and contact editing@geosociety.org with any questions.

We collected sediment samples from colddry (n = 106), temperate-dry (n = 22), and temperate-wet (n = 43) glacial environments, as well as hot-wet (n = 31) and hot-dry (n = 13)nonglacial settings. These samples represented primarily fluvial slack-water sediments, but they also included glacial drift, lake, and water-track sediment, as well as soils from both glacial and nonglacial systems. Soil profiles were sampled at 10–20 cm increments within the top \sim 10 cm to 1 m where possible. Table S1 provides complete sample descriptions and metadata on global positioning system (GPS) locations. All sediment samples were frozen until analysis. We also collected bedrock from Antarctica, Peru, Puerto Rico, and Anza Borrego and relied on published work for bedrock compositions of samples from Washington (Smith, 1903), Norway (Gordon et al., 2013), and Iceland (Kelly et al., 2014).

Antarctica

The McMurdo Dry Valleys are characterized as a largely ice-free polar desert, with MAT around -18 °C (within -14 °C to -30 °C temperature range) and MAP (mostly snowfall) of 100 mm/yr (Fountain et al., 1999; Doran et al., 2002, 2008). Nevertheless, chemical weathering occurs, as inferred from solute fluxes in meltwater streams (Nezat et al., 2001; Maurice et al., 2002; Gooseff et al., 2002; Stumpf et al., 2012; Lyons et al., 2015) and weathering products observed within rocks and soils (Guglielmin et al., 2005; Levy et al., 2014; Cuozzo et al., 2020). Fine-grained sediments produced by limited glacial grinding, as well as eolian redistribution of fine-grained glacial deposits, supply ample surface area for weathering reactions (Stumpf et al., 2012; Marra et al., 2017). Polyextremophilic microbial communities also likely contribute to nutrient and weathering fluxes, as well as reworking the sediments and changing their mineralogy and chemistry, as evidenced by scanning electron microscopy (SEM) images coupled with energy-dispersive spectroscopy (EDS) measurements (Demirel-

TABLE 1. SUMMARY OF THE FIELD SITE CHARACTERISTICS (CLIMATE CLASSES ARE ACCORDING TO KÖPPEN-GEIGER CLIMATE CLASSIFICATION*)

Field area	Latitude (°)	Longitude (°)	Bedrock	Climate	MAT (°C)	MAP (mm/yr)
Glacial McMurdo Dry Valleys, Antarctica Cordillera Blanca, Peru Jostedalsbreen, Norway Eyjafjallajökull, Iceland	77.24°S 9.01°S 61.59°N 63.67°N	162.48°E 77.69°W 6.99°E 19.63°W	Granite, granodiorite, hornblende-biotite orthogenesis Granodiorite, tonalite Quartz monzonite, granitic gneiss, granodiorite Basalt	Polar ice cap Cold, semiarid Subpolar oceanic Polar tundra	-18 8 4.5 3	100 588 1769 1000
Mount Stuart, Washington Nonglacial SE Puerto Rico Anza Borrego Desert, California	47.49°N 18.07°N 32.88°N	120.9°W 65.93°W 116.21°W	Granite, granodiorite Granodiorite, metavolcanics, diorite Tonalite	Subpolar oceanic Tropical rain forest Hot desert	8 22 23	1270 4200 150

Note: MAT—mean annual temperature; MAP—mean annual precipitation.

*Geiger and Pohl (1953); Beck et al. (2018).

Floyd et al., 2022). Poorly developed permafrost soils are mainly located on the valley slopes and floodplains, which are composed of drift deposits from previous cycles of glacial advance and retreat within the valleys (Campbell and Claridge, 2006; Bockheim and McLeod, 2008; Levy et al., 2011).

Taylor Valley

Eastern Taylor Valley is largely covered by the Last Glacial Maximum (LGM)—aged Ross Sea Drift, which contains clasts from the underlying granite and biotite orthogneiss, as well as basalt, sandstone, and dolerite clasts sourced from outside of the valley (Hall et al., 2000). The western portion of the valley is covered by drifts largely from Taylor glacier, an outlet of the East Antarctic Ice Sheet, which are also reworked by proglacial fluvial stream systems (Hall et al., 2000; Higgins et al., 2000).

Water Tracks

Water tracks are gully-like groundwater features with dark-toned surfaces. They have been attributed previously to briny groundwater activity (Levy et al., 2008, 2011); evaporation of the briny groundwater can lead to bright salt efflorescence on adjacent soils (Weidong et al., 2002). Water tracks are observed within dry ephemeral stream channels and along interchannel hillslopes and contribute to proglacial lake nutrient budgets by transporting weathering solutes. Therefore, water tracks are part of the hydrological cycle within Taylor Valley (Levy et al., 2011).

Wright Valley

The eastern end of Wright Valley is underlain by granite, quartz monzonite, and granodiorite bedrock (Brownworth and Denton plutons) and filled with pre-LGM drifts (Brownworth, Trilogy, Loke, Loop, Peleus, and various Alpine drifts) dating from the late Quaternary to as old as the Miocene that contain heterogeneous clasts from these bedrock types (Hall and Denton, 2005). Wright Valley soils are composed of these drifts, in addition to bedrock clasts of Ferrar Dolerite, Olympus granite gneiss, Vida granite, and microdiorite (Hall and Denton, 2005; Campbell and Claridge, 2006; Bockheim and McLeod, 2008).

Peru

The Llanganuco and Parón Valleys are at high elevation within the Cordillera Blanca mountain range, and they exhibit a cold and semiarid climate regime with highly seasonal precipitation (MAT = 0-9 °C; MAP = 800-1200 mm/yr) due to high elevation and El Niño–La Niña oscilla-

tions (Kaser et al., 1990, 2003; Vuille et al., 2008; Bury et al., 2011). Climate is heavily affected by the topography, where high peaks act as a barrier to moist air masses. The hydrological cycle during the dry season (June to September) consists of glacial streams and groundwater, but the water budget is reduced by sublimation (Vuille et al., 2008; Gordon et al., 2015). In contrast, rainfall is abundant from October to May. The wet season allows the western Cordillera Blanca glacial region to support vegetation in high-moisture soils that are underlain by lacustrine sediments and glacial till (Kaser et al., 2003; Baraer et al., 2015; Gordon et al., 2015). Llanganuco Valley is largely underlain by the granodioritic and tonalitic Cordillera Blanca batholith and locally by pyrite and sulfide mineral-rich marine black shales of the Upper Jurassic Chicama Formation, which is under ice cover (Wilson et al., 1995; Love et al., 2004), whereas the majority of the Parón Valley is underlain by Miocene batholith granodiorite complexes (Siame et al., 2006).

Norway

The Josteldalsbreen region has a cold and humid climate, with MAT of 4.5 °C and MAP of 1769 mm/yr. The glaciomorphological sediment and landforms locally record glacial advance and retreat during the Little Ice Age (LIA) of the late Holocene (Bickerton and Matthews, 1993; Lewis and Birnie, 2001). The Josteldalsbreen ice cap is located along the southwest coast of Norway, feeding S-NNW- and N-S-trending glacial valley streams that drain into lakes and fjords, including the Austerdalen and Langedalen Valleys we sampled. Precambrian acidic gneiss (granite to granodiorite composition), which is a part of the broader Norwegian Caledonides, underlies the western section of the Josteldalsbreen watershed (Rye et al., 1997). The bedrock composition and structure were affected by Precambrian and Caledonian orogenies, as well as ultrahigh- and highpressure metamorphism (Rye et al., 1997) referred to generally as the Western Gneiss Region (Root et al., 2005; Butler et al., 2015).

Iceland

Iceland is a volcanic island on the southern border of the Arctic Circle; it is underlain by volcanic rocks of 13 Ma to recent age. Silica-rich basaltic tephra eruptions have been frequent for the last 12,000 yr (Andrews and Eberl, 2007). MAT ranges between 0 °C and 4 °C, with MAP >600 mm/yr contributing to a humid climate that supports vegetation (Ólafsson et al., 2007). The Eyjafjallajökull volcanic eruption in 2010 (Sigmundsson et al., 2010) caused a catastrophic glacial outburst flood, which are common in the

region. Both the outburst floods and eolian processes (Arnalds et al., 2016) contribute to landform evolution and sediment budgets within the
fluvial catchments, as they rework former deposits and transport large amounts of fresh volcanic sediments (Prospero et al., 2012). Samples
for this study were collected in 2017 from the
outburst flood catchments of the Eyjafjallajökull volcanic eruption that occurred in 2010
(Table S1).

Washington

Mount Stuart is a glaciated peak within the Washington Cascades with a climate heavily affected by the topography, where high peaks act as a barrier to moist air masses (Reiners et al., 2003). MAP in the Northern Cascades region around Mount Stuart is 1500-2000 mm/ yr, and MAT is \sim 8–10 °C (based on PRISM group 30 yr annual precipitation and temperature maps; Daly et al., 1994, 2008). Erosion rates across the Cascades show similar trends as precipitation profiles, reaching a maximum of 0.33 mm/yr, which is correlated with fluvial discharge (Reiners et al., 2003). Mount Stuart is located on the Mount Stuart Batholith, a Late Cretaceous calc-alkaline pluton that intruded the metamorphic basement (pre-Cretaceous Chiwaukum Schist) of the Cascades (Erikson, 1977; Brown and Walker, 1993). The batholith varies spatially among tonalite, quartz diorite, granodiorite, granite, gabbro, and ultramafic rocks, locally intruded by mafic Tertiary dikes (Erikson, 1977). However, no mafic clasts or dikes were observed within the sampling area.

Puerto Rico

Southeastern Puerto Rico exhibits a hot and humid, tropical climate with MAT of 22 °C and MAP of 4200 mm/yr (Joo et al., 2018a, 2018b). Puerto Rico is commonly in the path of tropical storms and hurricanes, which induce landslides (Lepore et al., 2012; Besette-Kirton et al., 2019). The Rio Guayanés and Rio Guayabo watersheds in southeastern Puerto Rico are largely underlain by the Late Cretaceous San Lorenzo granodiorite, as well as quartz diorite and minor metavolcanics (Rogers et al., 1979). The granodioritic bedrock hosts thick layers of soil and saprolite (up to 1 m and 8 m, respectively; Fletcher et al., 2006; Murphy et al., 2012). At a larger scale, the field site lies within the Cordillera Central mountain range, which is largely underlain by Jurassic to Eocene igneous rocks (Monroe, 1980). The region is also tectonically active along the Puerto Rico Trench, characterized by 1 mm/yr uplift rates and moderate earthquakes (Mann et al., 2005).

Anza Borrego

The Anza Borrego Desert in the Sonoran Desert of Southern California has a hot and dry climate with MAT of 23 °C and MAP of 150 mm/ yr (Kottek et al., 2006; Joo et al., 2016). Rare, intense precipitation events result in ephemeral fluvial transport (Joo et al., 2016, 2018b). This watershed is largely underlain by tonalitic bedrock, within a larger region that also contains Jurassic metamorphic and Cretaceous plutonic units affected by activity along the Elsinore fault and uplift of the Peninsular Ranges Batholith (Remeika and Lindsay, 1992; Axen and Fletcher, 1998; Dorsey et al., 2011).

METHODS

Sample Processing and Characterization

To obtain the mud ($<63 \mu m$; silt + clay) silicate fractions of the sediment samples, we coned and quartered the thawed samples and then wet sieved for granulometry (total mud $\% < 63\mu\text{m}$, sand $\% < 63 \mu\text{m}$ –2 mm, gravel % > 2 mm). We treated the mud fraction with acetic acid overnight and H2O2 until the reaction (fizzing) ceased (2-5 d) to remove carbonate and organic constituents, respectively (Marra et al., 2017; Demirel-Floyd et al., 2022). Then, we measured the grain-size distribution of the muds using a Malvern Mastersizer 3000 laser particle size analyzer (LPSA), after treatment with sodium hexametaphosphate (Blott et al., 2004). Surface area of the muds was quantified using the Brunauer-Emmett-Teller (BET) nitrogen adsorption method (Brunauer et al., 1938).

We performed X-ray diffraction (XRD) analyses using a Cu radiation source, employing the Bragg-Brentano method (2°-70° 2θ angle interval with 0.02° step size and 2 s counting time, using fixed slits) on both random (bulk powder) and oriented (clay fraction) mounts. Clay minerals were identified both within random mounts and oriented mounts. Oriented mounts were prepared via filter-peel method, sonicating the mud slurry with detergent (sodium pyrophosphate), gravitationally settling the silt-sized grains via centrifuging at 800 rpm, and filtering the supernatant. Clay cakes collected on filters in this way were peeled on glass slides and air dried to prepare the oriented mounts. After scanning the air-dried peel, slides were subjected to ethylene glycol fumes overnight in a desiccator and immediately analyzed with XRD to determine the swelling type clays. Finally, slides were heat treated via baking at 550 °C for 1 h to determine any disappearing peaks to determine the presence or absence of kaolinite. Phase determinations were based on d-spacing values obtained

from these three-step scans, as well as modeling with the Clay SIM software (on selected samples) using the RockJock method (Eberl, 2003). We determined the quantitative mineral composition within the random mounts with MDI Jade software using the Reitveld refinement method (Bish and Howard, 1988), in combination with ClaySIM software using the RockJock method (Eberl, 2003). Major-oxide, rare earth element (REE), trace metal, and heavy metal chemistry of the samples was determined by the ALS Geochemistry (Reno, Nevada, USA), using inductively coupled plasma—mass spectrometry (ICP-MS) by Li borate fusion and acid-digestion methods.

Weathering Indices and Ternary Plots

We removed loss of ignition (LOI) data from the major-oxide results and normalized our data to 100% prior to any calculations or data transformations. We also corrected CaO values for apatite (Eq. 1) following Girty et al. (2013):

$$CaO^* = CaO - (3.3 \times P_2O_5).$$
 (1)

We calculated CIA as

$$CIA = \frac{Al_2O_3}{Al_2O_3 + CaO^* + Na_2O + K_2O} \times 100 (2)$$

following Nesbitt and Young (1982), and mafic-felsic-weathering (MFW) indices followed Ohta and Arai (2007) using molar ratios obtained from major-oxide analysis of the samples, as well as the chemical index of weathering (CIW; Harnois, 1988), plagioclase index of alteration (PIA; Fedo et al., 1995), and weathering index of Parker (WIP; Parker, 1970). In addition, we also generated Al $_2$ O $_3$ -(CaO + Na $_2$ O)-K $_2$ O, denoted A-CN-K, and A-CNK-(Fe $_2$ O $_3$ + MgO), denoted A-CNK-FM, and MFW ternary plots after normalizing the components of the plots to 100%. Note that the total iron for A-CNK-FM plots was reported as Fe $_2$ O $_3$.

Statistical Analyses on Sediments

Our data set consists of both categorical (depositional setting, location, climate regime) and numerical data (BET surface area, geochemistry, granulometry, LPSA, mineralogy, MAP, MAT). The data set also includes below detection limit (BDL) values that are susceptible to rounded zero errors (Martín-Fernández et al., 2003; Palarea-Albaladejo et al., 2014). The majority of the numerical data (geochemistry, mineralogy, granulometry) were also classified as compositional data, as they summed to 100% when considered as an independent data set, which can impose the constant sum problem (Aitchison, 1982; Aitchi-

son and Greenacre, 2002; Filzmoser et al., 2009; Grunsky et al., 2014). Multivariate statistical treatment is sensitive to issues such as rounded zeros and the constant sum problem within compositional data, biasing the results toward zero values (Aitchison, 1982; Aitchison and Greenacre, 2002). Therefore, we imputed (replaced) missing and BDL values as described below and applied log-ratio transformation methods to mitigate these potential issues prior to statistical analyses when necessary (Aitchison, 1982; Aitchison and Greenacre, 2002).

Below Detection Limit and Missing Data Imputations

We imputed BDL data (rounded zeros) and missing values using either multiplicative simple replacement (employed when <10% of data points were imputed by replacing the BDL data with a value of 65% of the analytical detection limit) or robust expectation-maximization (EM) algorithms (employed when >10% of the data points were imputed through replacement of missing data based on other observations within the same sample group) using the R software packages (Hron et al., 2010; Martín-Fernández et al., 2012; Palarea-Albaladejo et al., 2014).

BDL imputation for major oxides, trace metals, and REEs. Our major-oxide, REE, and trace metal data had less than 10% BDL data. Therefore, we applied multiplicative simple replacement, where the BDL data were initially introduced as 0 within our data frame and then substituted with 65% of the detection limit using the multRepl function of the zCompositions R package (Palarea-Albaladejo et al., 2014). Due to the differences in units, we applied this method to major-oxide data (%) separate from the REE and trace metal data (ppm).

BDL and missing data imputation for heavy metals. We removed Ag, Cd, and Tl from our data set due to each element having >85% of sample values listed as BDL. After this filtering, we imputed the missing data in the remaining heavy metal data set using the multReplus function of the zCompositions R package (Palarea-Albaladejo et al., 2014). Since our heavy metals data set also contained >10% BDL, we next applied a robust ilr-EM algorithm (Martín-Fernández et al., 2012), using the impRZilr function of the robCompositions R package that is used for data containing outliers (Hron et al., 2010; Palarea-Albaladejo et al., 2014). We applied this function separately to the data within each field site because the BDL data were imputed drawing from other observations in the data set, and individual components might have significant differences between field sites.

Data Transformations

We applied data transformations to data groups that would result in the constant sum problem prior to statistical analysis of each group of variables (mineralogy, major oxides, REEs, trace elements, and heavy metals, individually). If these variables were combined as inputs (i.e., a data set composed of geochemistry and surface area combined), we did not complete the transformation step because there was no longer a constant sum issue.

We transformed our compositional data with the centered log-ratio (clr) transformation, using the clr function of the compositions R package (van den Boogaart and Tolosana-Delgado, 2008). The clr transformation uses the geometric mean of the data set as a divisor, which is then converted to logarithm (Aitchison, 1982), resulting in collinear data (Filzmoser et al., 2009). We chose the clr method due to its widespread application in multivariate statistical analyses of geochemical data (i.e., Grunsky et al., 2014), superiority over the additive log-ratio (alr) due to alr being subjective to a single reference divisor (Filzmoser et al., 2009), and simplicity as compared to isometric log-ratio (ilr) (Grunsky et al., 2014).

Principal Component Analysis

We used GraphPad Prism 9 software to run principal component analysis (PCA) using the Kaiser rule (eigenvalues >1) method, where principal components (PCs) are automatically selected based on maximum explained variance. PCA runs included multiple types of analyses (e.g., geochemistry, LPSA grain size, mineralogy, and BET together in one data set), so they were not clr transformed, as the complete data set did not fall under the constant sum problem. However, we used the imputed and clr transformed data set when we ran PCA on individual compositional data sets (e.g., mineralogy, major oxides, REEs, trace elements, and heavy metals) separately.

Significance Testing and Correlations

We performed two-way analysis of variance (ANOVA) using GraphPad Prism 9 to compare the significance of differences between the means calculated for categorical groups of individual numerical data subsets (i.e., means of CIA values belonging to different climatic regimes), coupled with Tukey's multiple comparisons. The family-wise alpha threshold was set to 0.05, and analyses were run within 95% confidence interval. We acknowledge that the statistical analyses were affected by the lack of replicate measurements from each sample. However, having multiple samples within individual watersheds from each field site lessened these effects. Multiple samples collected from each

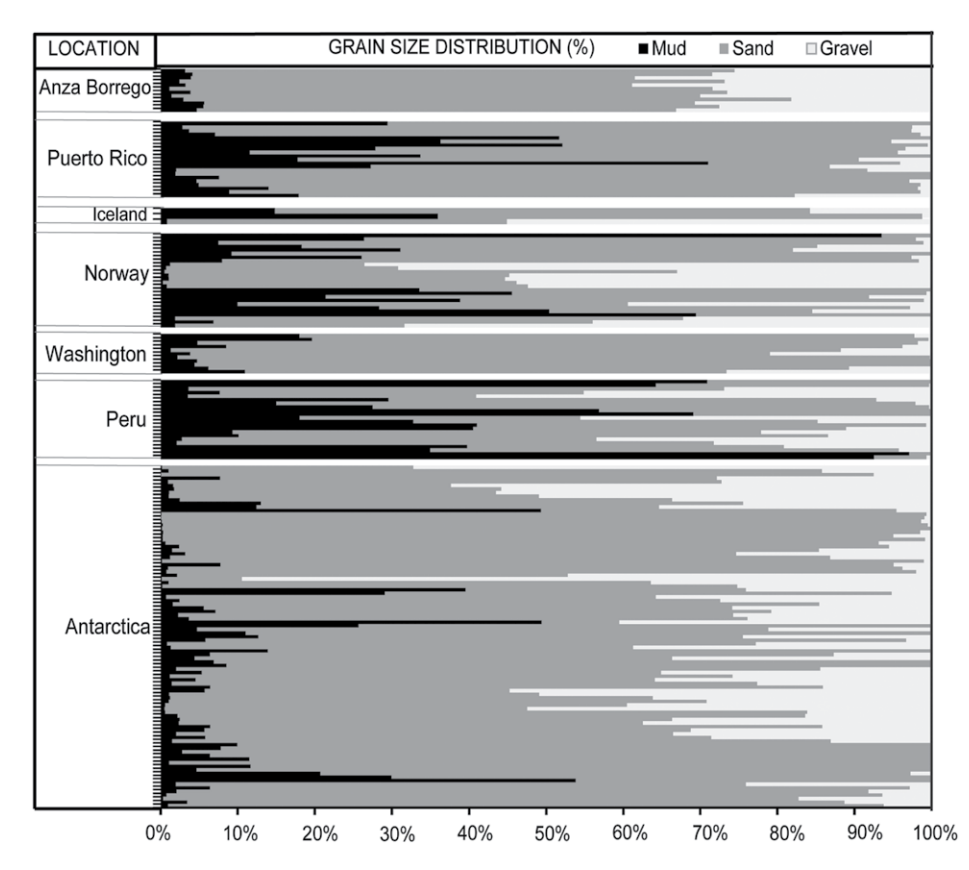


Figure 1. All granulometric data represented in a stacked area chart, showing % mud (<63 μ m, black), % sand (>63 μ m to <2 mm, dark gray), and % gravel (>2 mm, light gray) grain-size distribution within the bulk fraction of the samples. Antarctica sediments, except for a few glacial drifts, have the coarsest grain size within the bulk fractions. The y axis shows individual samples from indicated locations.

field site acted as replicates, as we were selecting our categories based on general field site conditions and climatic regime.

RESULTS

Grain Size

The granulometry data obtained from wet sieving and LPSA analyses are provided in Table S2 and illustrated in Figures 1-3. Proglacial lakes had the highest amount of mud ($<63 \mu m$ fraction, $\sim 97\%$) among all depositional settings, with samples from Peru exhibiting higher mud content than those from Norway (Table S2; Fig. 2). Peru soils and Puerto Rico saprolites were the other environments with high mud contents (Fig. 2), up to \sim 71%, within the bulk fraction. Note that, overall, Antarctic samples exhibited the lowest mud contents among the field areas, with the exception of some Anza Borrego soils (Fig. 2). However, anomalously high mud contents occurred within some proglacial fluvial, water-track, and

glacial drift samples from Antarctica (Fig. 2), where mud content reached 54% (Table S2).

As depositional settings influence grain-size distribution (via transport medium and energy, etc.), we focused on comparing the concentration of mud-sized grains collected from slack-water deposits within only fluvial settings (Fig. 2), the setting for which we had the most data across all field sites. Fluvial sediments from Norway (26.2%) had higher mud content on average, followed by Peru (25.1%), Iceland (17.2%), Puerto Rico (10.3%), Antarctica (7.2%), Washington (3.5%), and Anza Borrego (3.5%).

When we integrated the LPSA results with the overall granulometry data to calculate the fraction of clay-sized ($<4~\mu m$) sediment in the bulk samples, results varied significantly (Fig. 3). Summary statistics of clay-sized ($<4~\mu m$) sediment within the mud fraction of different depositional settings showed that proglacial lakes had the highest percentage of clay-sized ($<4~\mu m$) material (26%, n=4), followed by glacial drifts (19.7%, n=21), proglacial fluvial sediments (16.2%, n=94), soils (0-10~cm topsoil, 16.4%,

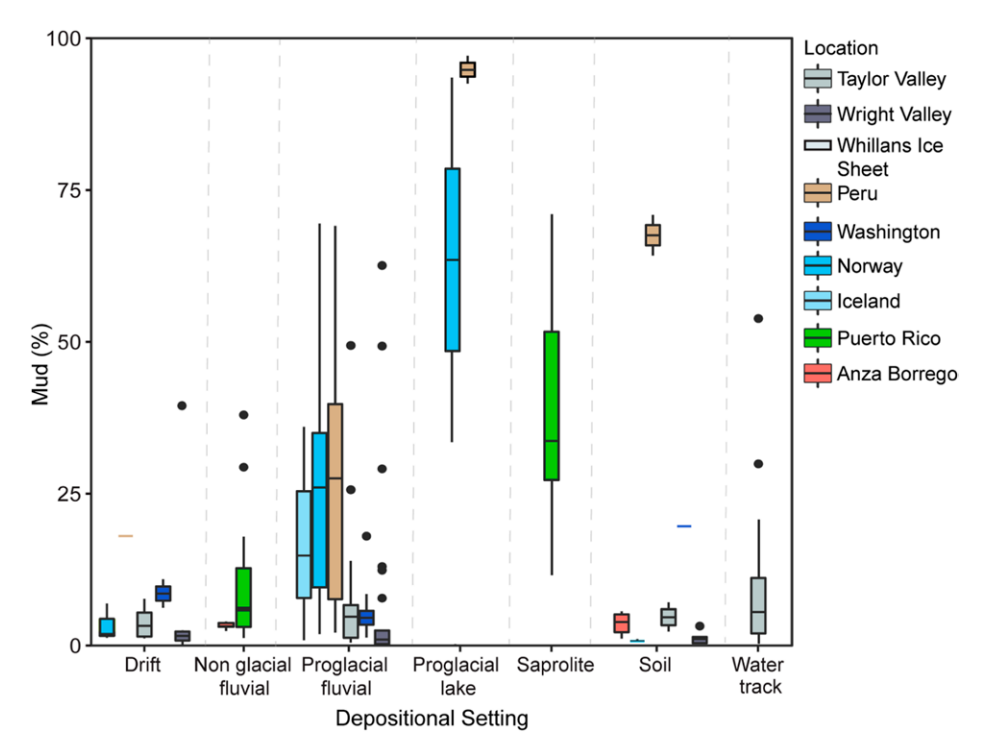


Figure 2. Box plots showing the percent distribution of mud-sized ($<63\,\mu m$) sediments within depositional settings at each field site, based on granulometry analysis of bulk fractions. There are no discernible trends of mud amount with climate (based on Table 1). Overall, proglacial lakes, saprolites, and Peruvian soils are the depositional environments with high amounts of mud-sized grains, followed by proglacial fluvial sediments, showing depositional setting is the overriding factor, masking any climatic trends.

n=7), water-track sediments (16%, n=18), nonglacial fluvial sediments (13.5%, n=17), and saprolites (8.3%, n=9).

In the comparison of the concentration of clay within the mud fraction of fluvial sediments collected in different field sites (Fig. 3), fluvial muds from Antarctica had the highest concentrations of clay-sized particles ($<4 \,\mu m$) on average (22.1%), followed by Anza Borrego (21.5%), Iceland (20.0%), Peru (13.4%), Puerto Rico (8.6%), Washington (4.9%), and Norway (2.7%).

Surface Area

Our BET surface area data from individual samples are provided in Table S2 and illustrated in Figure 4. Summary statistics of the BET results within different depositional settings showed that water-track sediments exhibited the highest surface area on average (32.9 m²/g, n = 18), followed by the nonglacial fluvial sediments (19.7 m²/g, n = 24), top layers of soil profiles (0–10 cm; 19.6 m²/g, n = 6), glacial drifts (18.0 m²/g, n = 22), saprolites (17.4 m²/g, n = 9), proglacial fluvial sediments (15.9 m²/g, n = 107), and proglacial lake sediments (4.0 m²/g, n = 4). Viewed across all field sites and

depositional settings combined (Fig. 4), Antarctic Taylor Valley samples had significantly higher BET surface area values than the other sites, with an average of 63.6 m²/g within the CAMP (Table S2) soil profile samples (n=4), followed by the proglacial fluvial sediments (39.3 m²/g, n=27), water tracks (32.9 m²/g, n=18), and glacial drifts (27.8 m²/g, n=7) (Table S2). Delta Stream sediments within the Taylor Valley proglacial watershed displayed anomalously high BET values (Fig. 4), reaching up to 70.6 m²/g (Table S2).

Mineralogy

Results of our quantitative XRD analyses are listed in Table S3 for each sample. Although we tried to keep the underlying lithology largely similar by targeting granitic to granodiorite composition bedrock sources (with the exception of Iceland), there were significant differences in the primary rock-forming minerals present in each field area (Fig. 5), which are also reflected in PCAs as individual clusters belonging to field sites plotting away from each other (Fig. 6). Summary statistics on individual field sites showed that Peru sediments contained the

highest average fraction of primary rock-forming silicates within the mud fraction (95.1%, n = 14), followed by Anza Borrego (85.2%, n = 5), Washington (64%, n = 11), Antarctica (64%, n = 58), Iceland (63.1%, n = 3), Norway (57%, n = 15), and Puerto Rico (56%, n = 23), in descending order. Clay mineral and miscellaneous secondary phyllosilicate mineral (serpentine, zeophyllite, pyrophyllite, clinozoisite) abundance (excluding primary mica minerals) followed an inverse order, as expected (except for Iceland), with Puerto Rico having the highest average secondary mineral content (43.4%), followed by Norway (42%), Antarctica (34.4%), Washington (25%), Anza Borrego (14.4%), Iceland (5%), and Peru (4.7%). Zeolites were only observed within glacial settings, where the highest concentrations were observed within Washington muds (8.5% on average), followed by Norway (0.9%), Antarctica (0.7%), Iceland (0.7%), and Peru (0.2%). Note that Iceland sediments contained on average 30% amorphous material. Remaining mineral fractions were accessory minerals for all sediments. Further details regarding the primary rock-forming and accessory minerals, as well as zeolites and amorphous phases, can be found in the Supplemental Material.

Clay Minerals

Secondary clay mineral assemblages (Table S3) within the Antarctic McMurdo Dry Valley muds collected from glaciofluvial and drift samples were dominated by illite, and they also contained abundant chlorite group minerals (clinochlore > chamosite), smectites (montmorillonite and amorphous smectites), mixed-layer clays (illite-smectite and chlorite-smectite), and, locally, small amounts of vermiculite. Montmorillonite was most abundant within water-track sediments. Vermiculite typically occurred in samples where biotite contents were relatively low. McMurdo Dry Valley permafrost soil samples contained varying illite and montmorillonite assemblages, where montmorillonite content was higher within the top 20 cm of the profiles in general, accompanied by relatively lower abundances of chlorite group minerals. Note that we did not detect kaolinite in our XRD analyses of McMurdo Dry Valley sediments, but kaolinite occurrences were previously reported within similar sediment samples from the Antarctic McMurdo Dry Valleys (Marra et al., 2017).

Secondary clays in Norway muds showed a similar assemblage, where illite predominated in the fluvial sediments, montmorillonite occurred in drifts and soils, and chlorite was observed in proglacial lake, proglacial fluvial, and drift sediments. Note that Norway muds had significantly higher illite concentrations (~40% illite)

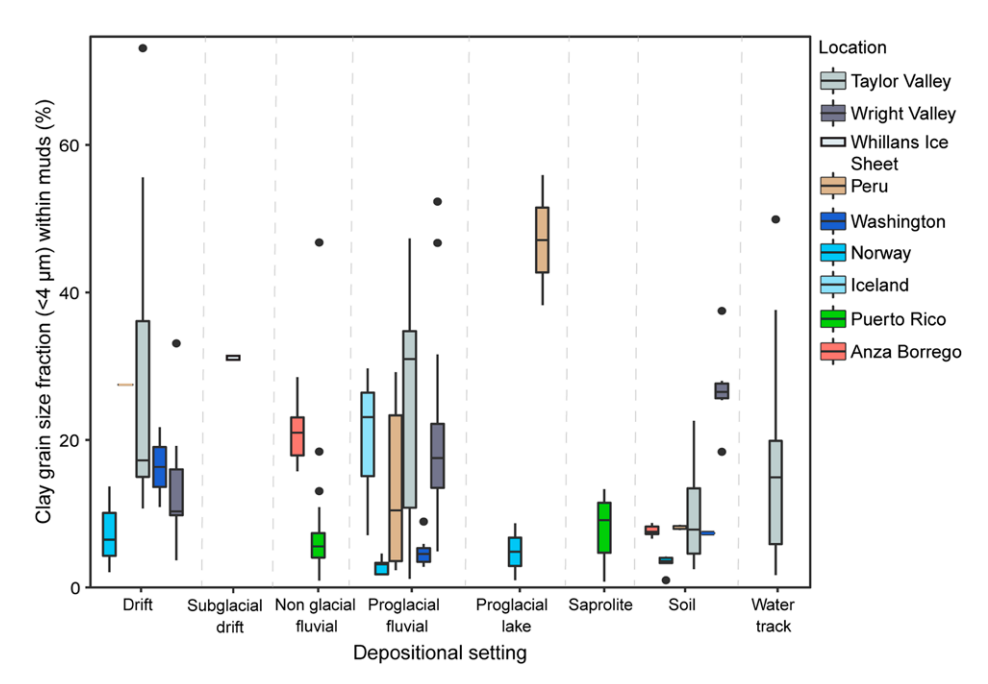


Figure 3. Box plots showing the percent distribution of clay-sized ($<4 \,\mu m$) grains within depositional settings at each field site, based on laser particle size analyzer (LPSA) analysis of mud fractions. Overall, Peruvian proglacial lakes, Wright Valley soils, and all Taylor Valley depositional environments are the settings with high amounts of clay-sized grains. Within fluvial setting, muds from Antarctica have higher concentrations of clay-sized particles ($<4 \,\mu m$) on average (22.1%), followed by Anza Borrego (21.5%), Iceland (20.0%), Peru (13.4%), Puerto Rico (8.6%), Washington (4.9%), and Norway (2.7%).

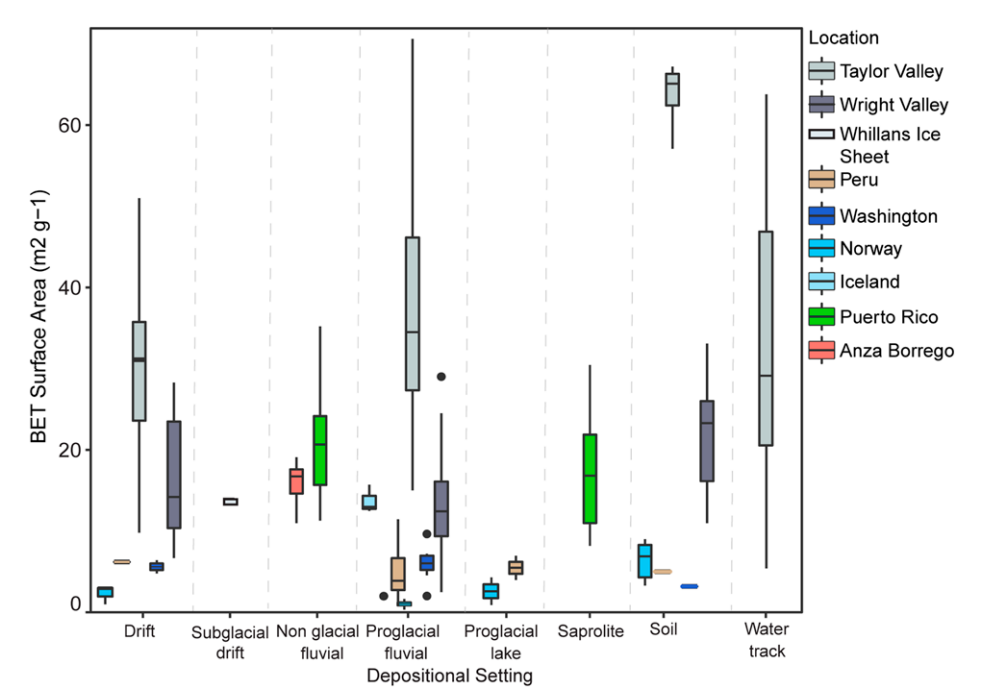


Figure 4. Box plots showing the distribution of grain surface area (m^2 g^{-1} , measured by Brunauer-Emmett-Teller [BET] method) of muds within depositional settings at each field site. The surface area of Antarctic Taylor Valley muds significantly exceeds other field sites within all depositional settings where data are available. There are no discernible trends of mud surface area with climate.

compared to the other field sites. Chlorite predominated in the relatively small concentration of clay minerals observed in Peru fluvial samples (clinochlore > chamosite), while palygorskite was also observed within proglacial lake sediments. Washington sediments were also enriched in chlorite minerals (mostly clinochlore) and had local occurrences of palygorskite, although montmorillonite and vermiculite were locally higher in abundance within meltwater stream sediments. Smectites predominated in the clay minerals observed in Iceland muds (montmorillonite and some amorphous smectite, as identified by the ClaySIM software).

The most distinctive difference in clay mineralogy observed between glacial and warmer climatic settings was the occurrence and abundance of kaolinite in Puerto Rico and Anza Borrego (Table S3). Puerto Rico sediment muds contained up to 93% of kaolinite (40% kaolinite on average), where the highest kaolinite concentrations were observed in saprolites. The only secondary clay mineral observed in Puerto Rico fluvial muds was kaolinite, whereas the saprolite also contained chlorite and vermiculite in lower abundances. Clay minerals observed in Anza Borrego muds, on the other hand, were dominated by illite, followed by kaolinite and smectite.

Note that we are defining illite as the mineral specimen that has a *d*-spacing value of 10 Å. Mechanical grinding of muscovite, which is especially pronounced in glacial sites via glacial grinding, also produces a 10 Å *d*-spacing value. Therefore, amounts of illite within the samples reported in Table S3, and illustrated in Figure 5, might be artifacts of mechanical grinding, as well as being secondary products of biotite weathering.

Sediment Geochemistry

Major-oxide results are reported in Table S4. We also analyzed heavy metals, trace metals, and REE concentrations, which can be found in Tables S5, S6, and S7, respectively. Overall, PCAs of major oxides, trace metals, heavy metals, and REE composition of the mud fraction samples (Fig. 7) illustrated overlapping compositions as well as distinctive differences between samples collected from different field sites. Washington (square) and Antarctic (asterisk) mud compositions overlapped, while fluvial Puerto Rico (circle) and Anza Borrego (triangle) samples clustered close to them. The Anza Borrego samples, however, displayed different heavy metal compositions than the Washington, Antarctica, and Puerto Rico sediments. After examining the entire suite of geochemical data (Tables S4-S7), the Puerto Rico saprolites, Norway muds, Icelandic basalts, and the

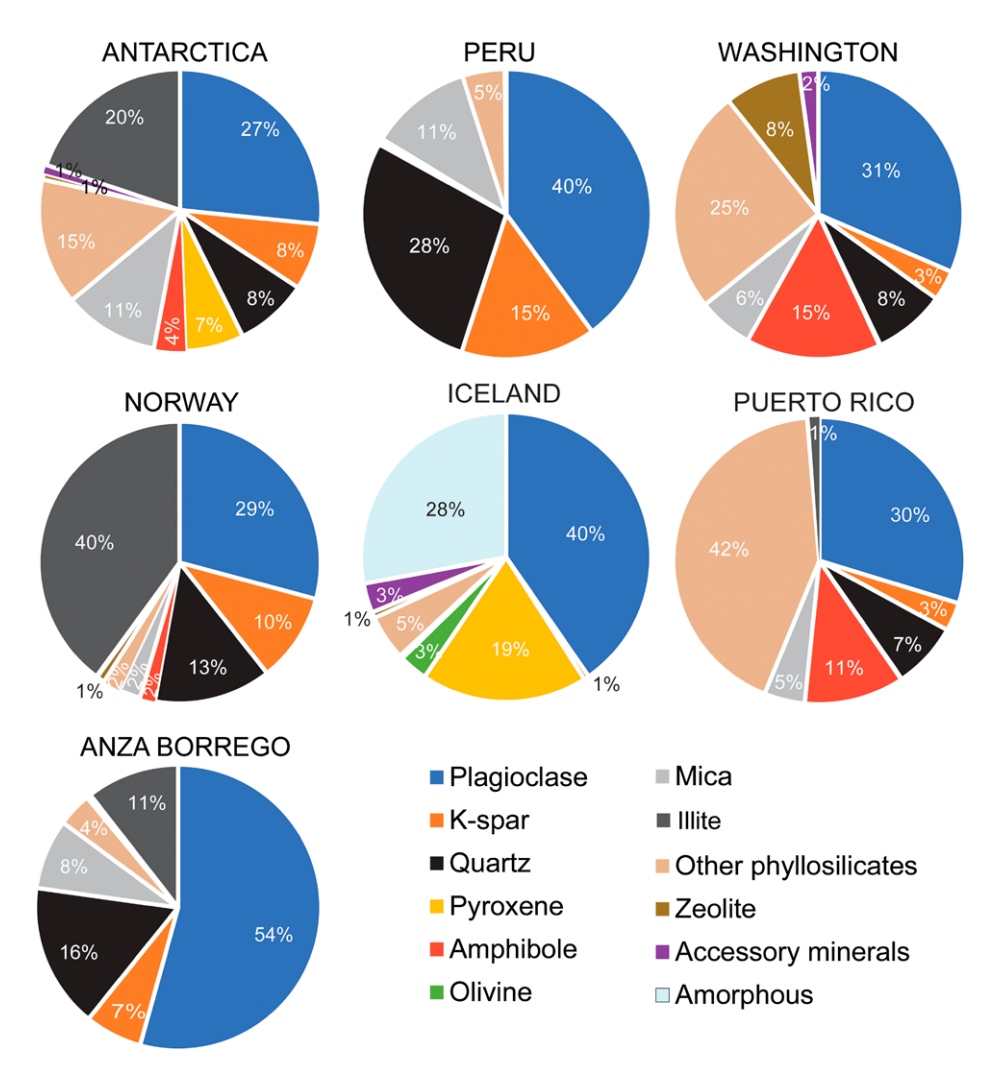


Figure 5. Pie charts illustrating the representative quantitative mineralogical compositions of muds from each field site, based on averaged values. Despite choosing field sites with similar underlying bedrock (except for Iceland), mineralogical composition of the muds varied significantly between field sites. Note that we are defining illite as the mineral specimen that has a *d*-spacing value of 10 Å. Mechanical grinding of muscovite, which is especially pronounced in glacial sites via glacial grinding, also produces a 10 Å *d*-spacing value. Therefore, amounts of illite illustrated in Figure 5 might be artifacts of mechanical grinding, especially pronounced in Norway mineralogy, as well as being secondary products of biotite weathering. K-spar—K-feldspar.

majority of the Peru sediments lie distinctively apart from the other samples on the PCA plots (Fig. 7), suggesting that they have significantly different chemical compositions compared to the other muds.

Figure S2 shows each individual major-oxide component plotted against SiO_2 (%) content of individual observations. We calculated average major-oxide concentrations for each field site normalized to average SiO_2 values (slopes within Fig. S2 calculated for individual field sites, e.g., Al_2O_3/SiO_2). Aluminum was significantly higher in Puerto Rico sediments ($Al_2O_3/SiO_2 = 0.52$) as compared to other field sites, followed by Ant-

arctica, Anza Borrego, and Iceland, which had similar Al_2O_3/SiO_2 ratios (\sim 0.3), whereas Washington, Norway, and Peru muds displayed lower Al_2O_3/SiO_2 values. Iron was significantly higher in Iceland basalts ($Fe_2O_3/SiO_2=0.24$) and significantly lower in Peru, Norway, and Anza Borrego sediments ($Fe_2O_3/SiO_2=0.04-0.07$), whereas the rest of the field sites had similar Fe_2O_3/SiO_2 ratios (0.16–0.2). We note that TiO_2 , Cr_2O_3 , CaO, C

ments displayed the lowest Na_2O/SiO_2 ratios $(Na_2O/SiO_2=0.04-0.05)$, relative to other fields, which had Na_2O/SiO_2 ratios of $\sim 0.06-0.07$. Washington, Iceland, Puerto Rico, and Anza Borrego had significantly lower K_2O/SiO_2 ratios $(K_2O/SiO_2=0.02-0.03)$, reflecting lower K-feldspar contents, relative to other field sites $(K_2O/SiO_2=\sim 0.05-0.06)$. Finally, Norway and Iceland muds had significantly higher P as compared to other field sites $(P_2O_5/SiO_2=0.011$ and 0.009, respectively), whereas Washington and Antarctica muds had moderate P_2O_5/SiO_2 values (0.007 and 0.006, respectively), and Puerto Rico, Anza Borrego, and Peru muds displayed the lowest P_2O_5/SiO_2 ratios (0.002-0.004).

Weathering Indices and Trends

All weathering index values are reported in Table S8, and average values for fluvial muds are reported in Table 2. In general, the weathering index trends were similar; therefore, we will focus primarily on CIA values in the remaining results and discussion. All CIA values fell between 46 and 99 (Table S8), and this range is considered to be indicative of incipient to extensive weathering, respectively, although CIA values are also influenced by source-rock lithology (Nesbitt and Young, 1982; Nesbitt et al., 1996, 1997). We focused primarily on the CIA values observed in the mud fraction of fluvial sediments, as these were the most abundant samples across all field sites, and they allowed us to directly compare trends within the same depositional system. We also discuss comparisons among depositional systems observed within field sites.

Icelandic fluvial muds had the lowest average CIA value (46), indicative of fresh basalt, whereas Puerto Rico fluvial muds exhibited values of ~66, and saprolites and soil exhibited averaged values of ~81, indicating strong weathering (Table S8). Both trends can also be seen on the A-CN-K ternary plot in Figure 8. Note that in the A-CN-K diagram (Fig. 8), Antarctica, Washington, Norway, Peru, and Anza Borrego data points overlap one another, with only Puerto Rico sediments distinctly illustrating an expected increasing weathering trend from bedrock to fluvial sediments to saprolite to soil, with values ranging from 55 to 96.

When we compared only the CIA values of fluvial muds (Table 2), the values were highest in Puerto Rico muds (62.2%), followed by Anza Borrego (60.6%), Peru (55.7%), Norway (53.2), Washington (52.1%), Antarctica (48.6%), and Iceland (46.4%). To reduce the provenance effect on chemical trends, we normalized average fluvial mud CIA values to average values of bedrock from each field site (Table 2). The order of the normalized CIA values (CIA_n) did

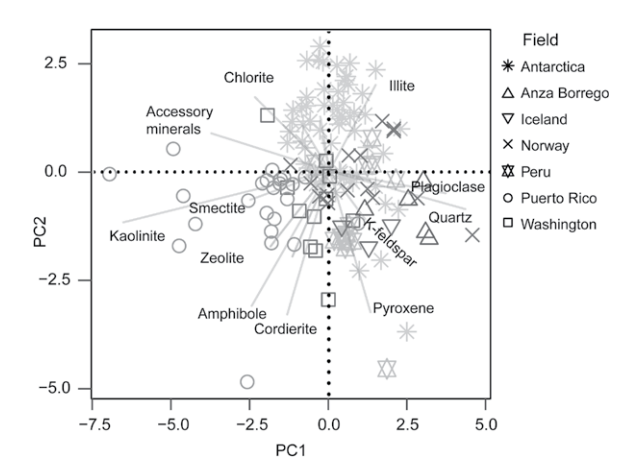


Figure 6. Principal component analysis (PCA) of the quantitative mineralogy of the muds from all field sites. Vectors represent loadings (variables) in PCA, and their magnitudes represent their relative significance in terms of the differences observed in mineralogy (i.e., higher magnitudes are more significant). Vectors pointing toward particular data points, or within the same quadrant, indicate that those data points significantly control the differences in concentration repre-

sented by the loading vectors. Note that we only labeled the significant vectors for clarity of illustration. The signs of the principal components (PC) are not representative of physical differences in the sample but are simply an artifact of the PCA process.

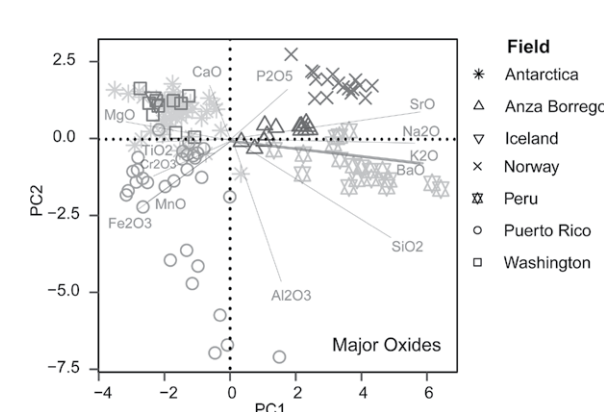


Figure 7. Principal component analysis (PCA) of the major-oxide chemistry of the muds from all field sites. Note that we only included loading vectors for major oxides, as major-oxide chemistry is the focus of the discussions.

not change, except for Iceland, demonstrating the effect of provenance in CIA values.

DISCUSSION

Controls on Grain Surface Area— Implications for Weathering and Climate

Sediment surface area reflects grain size and shape, as well as mineralogy and surface roughness. Therefore, both the concentration of claysized particles as well as the mineralogy and amount of secondary minerals influence surface area. Granulometry, mineralogy, and surface roughness are affected by weathering processes, including mechanical, chemical, and biological processes that vary significantly across different climatic regimes and depositional settings. Therefore, based on the hypothesis that the mineralogy and chemical composition of finegrained sediment, as well as physical properties (grain size, surface area, and texture) derived by weathering, are inherited from their depositional settings and climate, we investigated BET surface area and grain size as parameters that can inform interpretations of weathering and climate.

Theoretically, surface area should correlate inversely with grain size (Horowitz and Elrick, 1987) and increase in warmer, wetter settings owing to the production of abundant secondary clay minerals and iron (hydr)oxides attendant with chemical weathering (Velbel, 1993; White et al., 1999; White and Brantley, 2003). Surface area values for muds from warm climates in our data set, i.e., Anza Borrego (11-19.1 m²/g; hot, arid) and Puerto Rico (8.2-35.2 m²/g; hot, wet), followed this expectation, exhibiting higher surface areas than most of the glacially derived muds (0.3-70.6 m²/g), with the exception of muds from the Antarctic McMurdo Dry Valleys (2.5-70.6 m²/g; see below). The Anza Borrego fluvial muds contained abundant clay-sized particles (21.5%), and Puerto Rico muds on average contained a much higher concentration of clay minerals (\sim 43%; Fig. 5) than other field sites.

Within glacial settings, wet-based temperate glaciers produce abundant fine-grained material due to mechanical weathering associated with

basal sliding (Anderson et al., 1997; Anderson, 2005). Therefore, temperate glacial deposits are expected to have high surface areas attributable to the abundance of silt- and clay-sized glacial flour (Anderson et al., 1997). In contrast, coldbased glaciers, such as those in the McMurdo Dry Valleys, are not thought to produce abundant fine-grained sediments due to the lack of basal sliding. However, within the mud fraction, Antarctic sediments (especially from Taylor Valley, which is partially wet-based) exhibited the highest surface area, even exceeding those from tropical regions (e.g., Puerto Rico). McMurdo Dry Valley sediments contained less mud-sized material as compared to the majority of the field sites; however, McMurdo Dry Valley muds, particularly those from Taylor Valley, contained more clay-sized particles within the mud fraction than the other glacial sites. Therefore, one reason Antarctic muds exhibited the highest surface area values is that they contained abundant claysized particles. Marra et al. (2015) attributed the production and transport of high-surface-area sediments, as well as the significant variability observed within Wright and Taylor Valley streams, to variations in eolian input and stream discharge rates, as well as the sediment properties within underlying drifts and potentially enhanced weathering due to microbially produced organic acids. Fine-grained sediments are also concentrated onto glacial surfaces (where they may undergo weathering) and released into the stream channels during melting during the austral summer (Marra et al., 2015).

The high BET surface areas observed in the Antarctic mud samples is surprising (Fig. 4; Table S2), as one would expect a tropical region saprolite sample that is almost completely composed of clay minerals (e.g., Puerto Rico PM-RG-SAP-6A sample with BET = $21.9 \text{ m}^2/\text{g}$, ~93% kaolinite; Tables S2 and S3) to exhibit the highest surface area within the entire data set. However, Antarctic sediments had higher smectite content, potentially due to inheritance from marine sediments (Robert and Kennett, 1992, 1994, 1997), weathering of volcanic clasts and ash inherited from Mount Erebus and other Ross Sea region volcanoes (Ugolini, 1967), and older ages (potentially exposing grains to multiple cycles of weathering) compared to Anza Borrego and Puerto Rico muds, as well as other samples. Smectites have some of the highest BET surface areas among the wide range of Clay Mineral Society standards (Table S9; Dogan et al., 2006, 2007). Therefore, the relatively high smectite content of most of the Antarctic samples (Table S3) likely contributed to the anomalously high surface area values measured in these samples.

Sediment age also affects the chemical, mineralogical, and physical weathering signatures,

TABLE 2. WEATHERING INDEX VALUES FOR FLUVIAL MUDS AND BEDROCK AND BEDROCK-NORMALIZED VALUES, ON AVERAGE, FOR EACH FIELD SITE

Sample	CIA*	CIW [†]	PIA§	WIP#
Antarctica Fluvial mud Bedrock Mud/bedrock	48.6 (4.0) 47.9 1.01**	52.9 (5.1) 54.7 0.97	48.5 (4.6) 47.8 1.01	72.4 (2.1) 76.6 0.95
<u>Peru</u> Fluvial mud Bedrock Mud/bedrock	55.7 (2.5) 51.0 1.09**	64.1 (3.2) 59.7 1.07	57.7 (3.4) 51.4 1.12	71.9 (5.7) 79.4 0.91
<u>Washington</u> Fluvial mud Bedrock Mud/bedrock	52.1 (1.8) 50.4 1.03**	55.1 (2.3) 54.3 1.01	52.4 (2.1) 50.4 1.04	65.7 (0.3) 74.4 0.88
<u>Norway</u> Fluvial mud Bedrock Mud/bedrock	53.2 (0.5) 51.2 1.04**	61.6 (1.4) 53.5 1.15	54.5 (0.8) 51.4 1.06	74.9 (3.0) 77.2 0.97
<u>lceland</u> Fluvial mud Bedrock Mud/bedrock	46.4 (0.2) 42.2 1.1**	48.3 (0.0) 43.2 1.12	46.1 (0.2) 41.9 1.1	71.4 (1.1) 76.3 0.94
<u>Puerto Rico</u> Fluvial mud Bedrock Mud/bedrock	66.2 (14.3) 43.9 1.51**	68.6 (14.7) 45.3 1.51	67.6 (14.6) 43.6 1.55	45.7 (10.7) 70.3 0.65
Anza Borrego Fluvial mud Bedrock Mud/bedrock	60.6 (1.7) 51.9 1.17**	65.9 (2.5) 55.4 1.19	62.7 (2.3) 52.2 1.2	63.3 (1.8) 61.6 1.03

Note: CIA—chemical index of alteration; CIW—chemical index of weathering; PIA—plagioclase index of alteration; WIP—weathering index of Parker. CaO values were corrected for apatite (Eq. 2) following Girty et al. (2013). Standard deviations for muds are given in paratheses.

including the surface area (White et al., 1996; Egli et al., 2001). Antarctic McMurdo Dry Valley sediments (ranging from LGM to Miocene age; Hall et al., 2000; Hall and Denton, 2005) are older than the other sediments we investigated, which were otherwise all first cycle. The Antarctic sediments may have experienced more than

one cycle of weathering owing to multiple glacial advances and retreats and freeze-thaw cycles as progressively older drifts were reworked and overprinted (Anderson et al., 1997; Hall et al., 2000; Hall and Denton, 2005), providing multiple opportunities to further develop secondary weathering products and associated high

surface area (White and Peterson, 1990; White et al., 1996). However, BET surface area values observed in the LGM-aged Taylor Valley samples significantly exceeded values observed in older Wright Valley sediments, suggesting that sediment age is not the primary factor controlling the variability in the surface area of these deposits; rather, the heterogeneous basal regimes of Taylor Valley glaciers, which included the wet-based Ross Sea drift, produced significant amounts of fine-grained material.

To quantitatively investigate the effects of climatic parameters (MAP and MAT) on BET and % clay grain size fraction observed in fluvial sediments across all field areas, we investigated correlations between these variables by constructing cross-plots (Fig. 9). Results indicated that relationships between BET and grain size with MAT and MAP are relatively weak and cannot be used individually as parameters to interpret climate, even though BET and grain size are by-products of weathering of the source material (Fig. 9). Therefore, our results indicate that climate is not a primary determinant of BET surface area and % clay in fluvial sediments (Fig. 9).

Effects of Provenance

Despite selecting field areas underlain by broadly similar granitoid bedrock, we observed distinct differences in the chemistry of mudsized ($<63 \, \mu m$) sediments; however, these differences appeared to have little to no link to climate. Indeed, the CIA values (Table 2; Table S8) and compositions plotted in A-CN-K space largely overlapped (Fig. 8), except for the saprolite and soil samples from Puerto Rico, which produced a strong chemical weathering

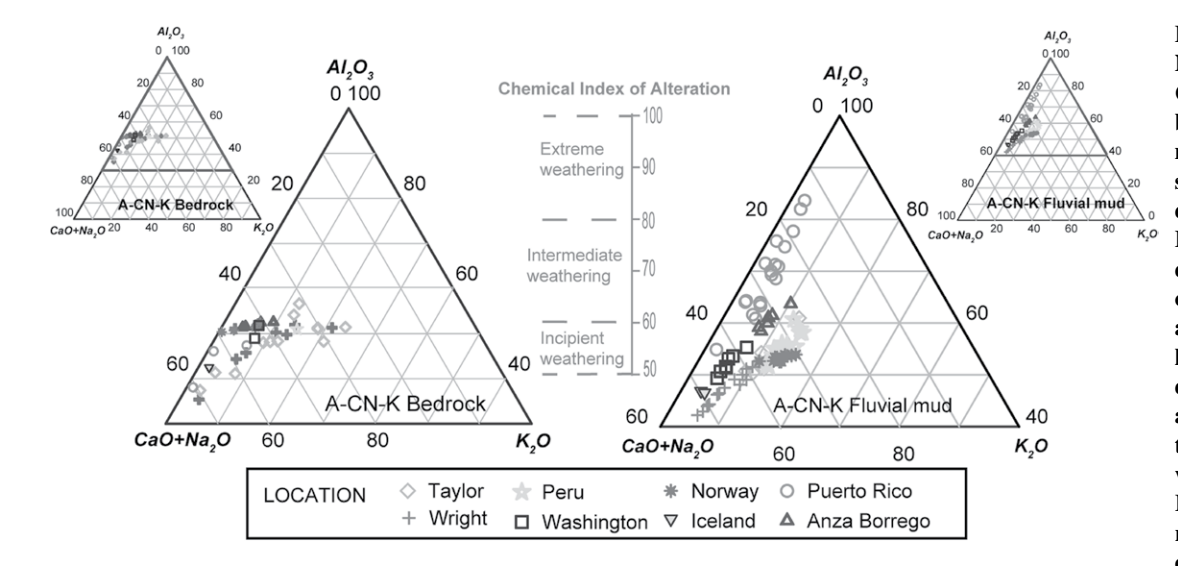


Figure 8. Al_2O_3 -(CaO + Na₂O)-K₂O, denoted A-CN-K, ternary plots of the bedrock (left) and fluvial muds (right) from all field sites. We zoomed on the data points for scaling. Locations of the bedrock data points are indicative of fresh bedrock, except for a few Antarctic Taylor Valley samples. Geochemical data collected from almost all locations show incipient to intermediate chemical weathering, while Puerto Rico muds show a trend ranging from incipient to extreme weathering. Except

for Puerto Rico muds, there are no discernible weathering trends between climatic regimes, as the muds ranging from cold to hot climates cluster together in the same region of the diagram.

^{*}Nesbitt and Young (1982).

[†]Harnois (1988).

[§]Fedo et al. (1995).

[#]Parker (1970).

^{**}Mud/bedrock values only under the CIA correspond to CIA_n = (CIA_{mud}/CIA_{bedrock}) as defined in the text.

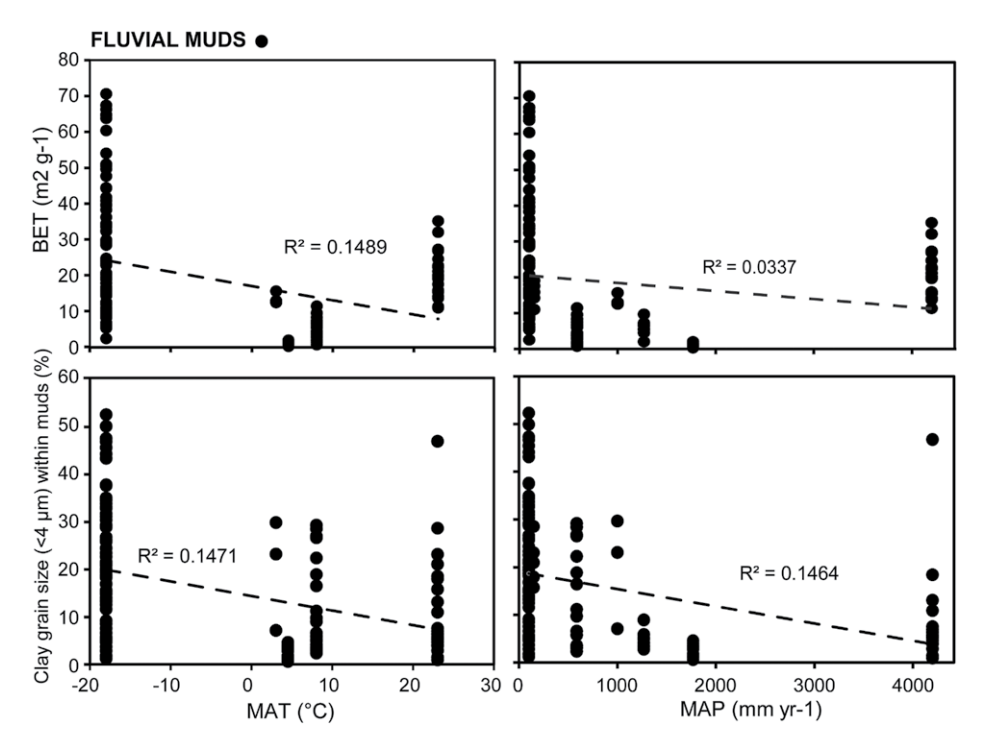


Figure 9. Correlation of Brunauer-Emmett-Teller (BET)-derived surface area and clay grain-size fraction within muds with mean annual temperature (MAT) and mean annual precipitation (MAP), based on fluvial samples. R^2 values suggest that there are no strong correlations between these variables.

signature (Figs. 5-8; Tables S3-S7). We also observed differences in both primary and secondary minerals among all field sites (Fig. 5). Mineralogical differences are commonly tied to climate and weathering, but they might also reflect subtle differences in provenance (Nesbitt et al., 1996; Ren et al., 2019; Mangold et al., 2019). For instance, low abundance of feldspar is often associated with the extent of weathering and linked to higher CIA values (Nesbitt and Young, 1982). However, variations in feldspar content and composition can also reflect provenance, leading to misinterpretations (Mangold et al., 2019). On the other hand, zeolite and clay minerals are associated with weathering conditions (weathering solute composition, weathered material, etc.) and climate (i.e., Barshad, 1966; Dickinson and Rosen, 2003; Wise, 2005; Jacobson et al., 2015), although linking their presence and abundances to certain climatic regimes is far from straightforward. Here, we observed zeolites only in the glacial muds within our data set, and their occurrences have previously been associated with low-temperature weathering of volcanic and plagioclase-rich rocks (i.e., via brines in Antarctica; Dickinson and Rosen, 2003). However, they also can form via other mechanisms (Wise, 2005), such as low-grade metamorphism of basalt in Iceland (i.e., Jacobson et al., 2015).

Speciation of clay minerals is also often tied to climate and weathering conditions. For instance, the presence of Fe/Mg-bearing smectites on Mars is often linked to alkaline pH and long-term wet conditions (Ehlmann et al., 2011), or weathering of basalts by acidic hydrothermal solutions (Peretyazhko et al., 2016) and/or the introduction of wet conditions to a previously dry environment (Bishop et al., 2018) in alternative perspectives. However, Antarctic smectites may also have been inherited from marine sediments during alternating wetdry periods (Robert and Kennett, 1992, 1994, 1997) or sourced from weathering of volcanic clasts and ash from Mount Erebus (Ugolini, 1967). Kaolinites are also linked to climate, where kaolinites are expected to form in areas with high precipitation and hot-humid climate regimes such as Puerto Rico, reflecting leaching of more soluble ions out of the system (Biscaye, 1965; Barshad, 1966; White et al., 1996, 1998; White and Buss, 2014; Joo et al., 2018a; Webb et al., 2022). However, though we did not observe kaolinites in our XRD analysis of Antarctic sediments (potentially owing to amounts below the detection limit), other studies have reported kaolinite within Antarctic sediments (Robert and Kennett, 1992, 1994, 1997; Marra et al., 2017). This suggests that, although minerals can be linked to specific climatic regime,

and CIA is widely utilized in paleoclimate studies (i.e., Nesbitt and Young, 1982; Soreghan and Soreghan, 2007; Goldberg and Humayun, 2010; Xiao et al., 2010; Bahlburg and Dobrzinski, 2011; Yang et al., 2016; Ren et al., 2019; Wang et al., 2020; Deng et al., 2022), paleoclimate interpretations are more complicated due to the ambiguity of the origin of most minerals and complicated climatic history of aged sediments (Thiry, 2000).

The A-CNK-FM diagram in the right block of Figure 10 shows that, with the exception of the Puerto Rico samples, only a few Peru mud samples and a single Norway sample trended significantly toward the weathering apex (toward A). Similar trends observed on the A-CN-K diagram (Fig. 8) indicate that only the Puerto Rico muds exhibited strong weathering trends. However, since the A-CNK-FM plot also incorporates Mg and Fe contents, it provides additional provenance information. The distribution of samples relative to the line that connects the FM apex and the point halfway between A and CNK likely reflects differences in provenance between samples (Nesbitt et al., 1996). We observed that Norway and Peru bedrock samples plotted toward the felsic apex, and Iceland bedrock plotted toward the mafic apex (as expected), whereas the underlying bedrock in Antarctica, Washington, Anza Borrego, and Puerto Rico plotted as mixed felsic-intermediate compositions. These differences indicate that, while we attempted to normalize for bedrock by targeting areas underlain by graniticgranodioritic compositions, even relatively small differences in lithology can result in significantly different bulk compositions as visualized in these ternary spaces and also as indicated by the significant differences in major-oxide chemistry and primary mineralogy (Figs. 6 and 7).

We also plotted the compositional data on a MFW diagram (Fig. 11; Ohta and Arai, 2007) to further investigate the role of provenance in the mud chemistry and weathering trends. In contrast to the A-CNK-FM plot, fluvial samples from Iceland, Antarctica, Washington, and Puerto Rico plotted closest to the mafic apex, while Peru samples plotted closest to felsic, and Norway and Anza Borrego samples were mostly in the felsic-intermediate range. Note that the Antarctic Taylor Valley drifts (mainly Ross Sea Drift) contained up to \sim 17% mafic clasts from the Ferrar Dolerite and McMurdo volcanics; however, the rest of the clast composition $(\sim 83\%)$ was largely granitic and granodioritic within the bulk fraction (Hall et al., 2000), suggesting that significant sorting effects cause the Antarctic muds to plot within the mafic apex (Nesbitt et al., 1996; von Eynatten et al., 2012). Only the Puerto Rico soil and saprolite samples plotted near the weathered apex (Fig. 11),

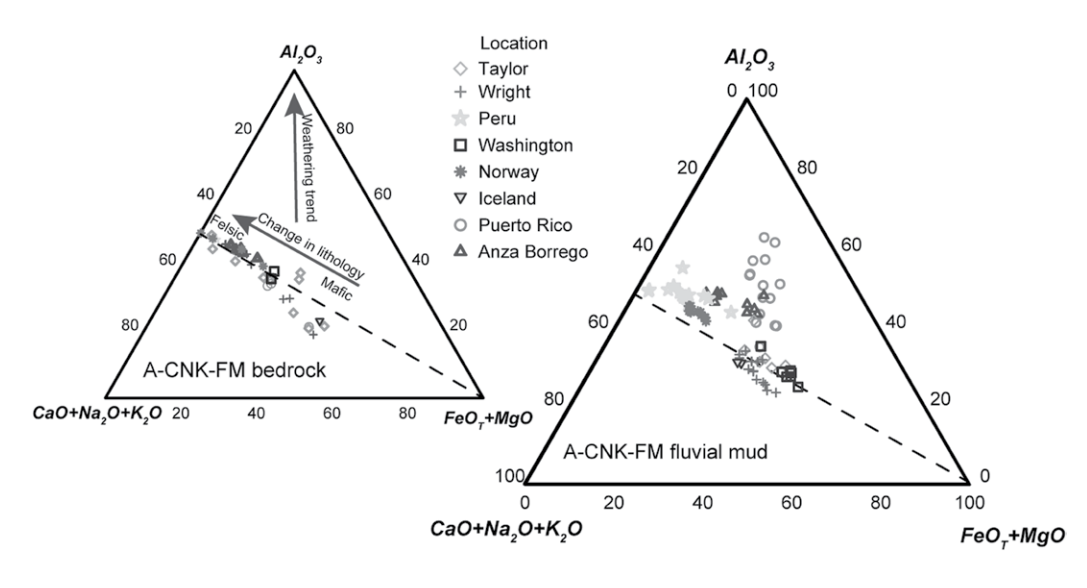


Figure 10. Al_2O_3 –(CaO + Na₂O + K_2O)– $(Fe_2O_3 + MgO)$, denoted A-CNK-FM, ternary plots of the bedrock (left) and fluvial muds (right) from all field sites. Variations along the dashed line indicate differences in lithology, changing from mafic to felsic in the arrow direction on the bedrock plot. Lithology is also variable within the fluvial muds, showing that Peru, Norway, and majority of the Anza Borrego muds are felsic, while a few Anza Borrego and Peru muds show intermediate composition. Antarctica and Washington and some Puerto Rico data points show intermediate-mafic composition,

plotting close to Iceland muds. Puerto Rico muds as well as a few Antarctica, Peru, and Norway muds show weathering trends, approaching the A apex.

consistent with the A-CN-K plots (Fig. 8) showing weathering trends only in the Puerto Rico samples. These results demonstrate that, among our end-member climate samples, MFW plots only indicate significant weathering signatures in tropical watersheds (i.e., Puerto Rico). However, CIA values and clay mineral assemblages indicative of moderate to intense weathering were also observed in Antarctic samples (Table 2; Table S8).

Further comparison of depositional settings within individual field sites (Fig. 11) revealed that soil and saprolite samples tended to show more intense weathering signatures than bedrock or fluvial samples, except for soils collected in Washington and Anza Borrego, which produced weathering indices that imply that they were less weathered than fluvial samples from the same watershed. Among Antarctic samples, we also observed that some bedrock and drift samples produced weathering indices that were higher than those observed in the soils, and the watertrack samples overlapped with soils (Levy et al., 2011). In addition, felsic bedrock from Antarctica and Puerto Rico (granite and granodiorite) plotted as mafic on the MFW plot, within the same region of the diagram as Iceland basalts, indicating that MFW plots may also produce misleading representations of lithology and provenance, in addition to being less sensitive to potential weathering trends.

Limitations of Ternary Diagrams for Fine- Grained Sediments

A-CN-K diagrams are generated using the Al₂O₃, CaO, K₂O, and N₂O contents of samples,

and they are often combined with CIA values to interpret weathering trends (Nesbitt and Young, 1982). A-CN-K plots were developed for, and are therefore more applicable to, chemical weathering in felsic-intermediate lithologies, since mafic lithologies also contain abundant FeO, MgO, MnO, Cr₂O₃, and TiO₂. Ignoring these more mafic components can obfuscate interpretations of weathering trends in mafic planetary settings (i.e., Martian regolith; Siebach et al., 2017; Berger et al., 2020), as well as within our mixedsourced (Antarctic) terrestrial muds. In contrast, A-CNK-FM diagrams account for FeO and MgO, and MFW diagrams incorporate all of the major-oxide components of the samples, removing the bias toward felsic components. However, these plots also produced surprising results that call into question the effectiveness of these tools as indicators of climate: (1) sediments from significantly warmer and wetter climates had CIA values comparable to Antarctic sediments and plotted in the same region on the A-CN-K diagram; (2) other than the Puerto Rico saprolites, samples with relatively high CIA values did not plot toward the weathered apex in MFW space; and, finally, (3) Puerto Rico sediments derived from intermediate bedrock and felsic-intermediate Antarctic sediments both plotted squarely in the mafic apex of MFW diagrams.

We posit that the discrepancies among the ternary plots of the muds we investigated, and the bulk bedrock lithology and observed mud mineralogy sampled from field sites within various climatic regimes (Figs. 9, 11, and 12), reflect the significant influence of CaO content on the weathering calculations. Minerals containing high abundances of CaO—particularly pla-

gioclase, amphibole, and pyroxene, which are largely generated from mixed bedrock compositions-become concentrated within the fine fraction due to physical sorting mechanisms. This produces higher concentrations of more mafic minerals within the mud fraction (Nesbitt et al., 1996; von Eynatten et al., 2012; McLennan et al., 2014; Siebach et al., 2017; Hurowitz et al., 2017; Bedford et al., 2019), skewing the ternary plots toward the mafic apex. We observed that this grain-size sorting effect was most prominent for sediments generated from intermediate and mixed bedrock compositions (such as Antarctic McMurdo Dry Valley sediments within our study), and we acknowledge that the sorting trends may be reversed in Icelandic sediments (less mafic content accumulating in finer size fractions) as reported by Thorpe et al. (2019).

For example, CaO is a major component in all three ternary plots, as well as being a primary variable in CIA calculations. The CaO values reported on the diagrams and included in the CIA calculations are representative of CaO within the siliciclastic components of the sediments, since we removed carbonates prior to the analyses and calculated CaO* values, which corrects CaO content to remove apatite (Eq. 2; Girty et al., 2013). While other secondary minerals, including sulfates, can also contribute to elevated CaO contents in fine-grained sediments (McLennan et al., 2014; Hurowitz et al., 2017; Bedford et al., 2019; Mangold et al., 2019), we detected no evidence of gypsum or other sulfates in our samples, and any secondary salts or carbonates were removed in our pre-analysis wet sieving, acid, and peroxide treatments. However, CaO content can be elevated owing to provenance;

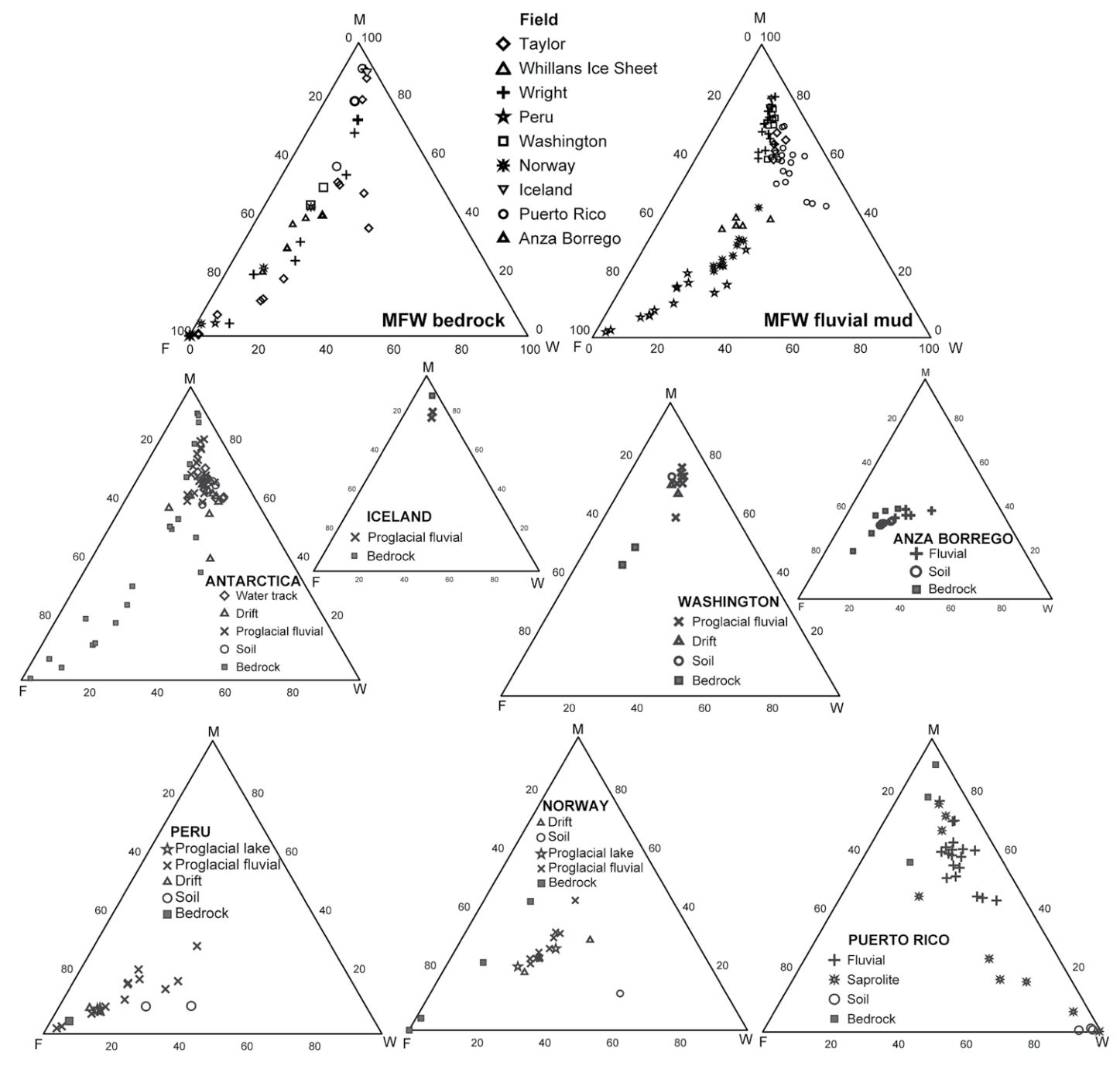


Figure 11. Mafic-felsic-weathering (MFW) ternary plots of the bedrock (left) and fluvial muds (right) from all field sites (top two plots). We additionally plotted MFW for individual field sites, illustrating various depositional settings of muds with different shapes (bottom). Individual investigations of depositional settings within each field site showed that soil and saprolite samples tend to show weathering trends, except in Washington and Anza Borrego, where soil samples plot as less weathered than fluvial samples. The most obvious weathering trend is observed in Puerto Rico samples, in agreement with Al_2O_3 –(CaO + Na_2O)– K_2O (i.e., A-CN-K) and Al_2O_3 –(CaO + Na_2O)– K_2O) (i.e., A-CNK-FM) plots (Figs. 8 and 10). We additionally noted that felsic bedrock plotted as mafic in Antarctica and Puerto Rico, suggesting limitations for both provenance and weathering interpretations.

for example, elevated anorthite compositions in a plagioclase-rich bedrock would produce lower CIA values, even when the extent of weathering is comparable among field sites (Mangold et al., 2019). Thus, the effects of physical sorting, e.g., concentrating CaO and other mafic oxides within the mud fraction (i.e., Nesbitt et al., 1996), could explain why samples derived from predominantly felsic and felsic-intermediate lithology plot close to the mafic apex in MFW diagrams. Mafic minerals are also more susceptible to physical and chemical weathering than more felsic minerals (Goldich, 1938). These processes concentrate more mafic minerals in finer-size fractions, whereas the felsic mineral content

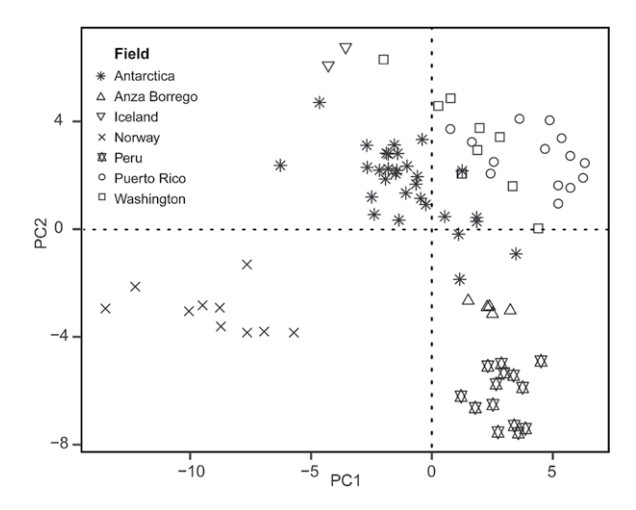


Figure 12. Principal component analysis (PCA) of all variables (mineralogy, grain size, % clay $<4~\mu m$, surface area, geochemistry). The signs of the principal components (PC) are not representative of physical differences in the sample but are simply an artifact of the PCA process. Overall, no significant trends were observed with climate. Instead, the data clustered with respect to provenance.

prevails in coarser sediment fractions (Nesbitt et al., 1996; von Eynatten et al., 2012). This influences the composition of fine-grained sediments eroded from mafic rocks (Siebach et al., 2017), but the trend is more pronounced in intermediate- and mixed-sourced sediments, where mafic minerals have relatively low concentrations in the bulk sediment but are heavily concentrated in the fine-grained fraction. In the case of intermediate- and mixed-source sediments, the regions that have higher abundances of Carich pyroxene (e.g., Antarctica) and amphibole (e.g., Washington) within the bedrock, as well as the regions with pronounced mechanical weathering (i.e., pulverization within glacial settings), are particularly susceptible to relative enrichment of mafic grains within the mud fraction, which could explain why these regions plot as mafic in the MFW plots.

The relative enrichment of metal oxides (Fe-, Mn-, and Ti-oxides) within the mud fraction via preferential weathering and sorting of mafic minerals could also contribute to pushing samples toward the mafic apex of the MFW diagram. Antarctic and Washington muds were notably rich in Fe₂O₃, MnO, and TiO₂, with concentrations comparable to Iceland muds, and their average Cr₂O₃ concentrations even exceeded Iceland basalts (Table S4). However, fluvial Puerto Rico muds derived from felsicintermediate granodiorite also plotted as mafic, potentially due to their relatively high Fe₂O₃ and MnO contents (\sim 10% and 0.19%), which were concentrated within the fine fraction. These iron and manganese concentrations are similar to those observed in the mixed-source Antarctic $(\sim 10\%$ and 0.16%) and basaltic Iceland muds (\sim 12%). Note that Joo et al. (2018a) reported up to 1.4% Fe-oxides based on XRD analyses within similar samples collected from Puerto Rico. We posit that the source of the Fe and Mn within Puerto Rico muds is likely secondary

oxides that are concentrated in soils by chemical weathering within a tropical climate (Huang et al., 2016; Nguyen et al., 2019). These Fe- and Mn-rich soils are delivered to the fluvial system via slope failure or storm events that preferentially transport soil to fluvial systems (Webb et al., 2022), including the B horizon, which is commonly enriched in metals leached from the horizon above.

Separating Weathering Signatures from Provenance to Interpret Climate

Ternary diagrams of weathering parameters are commonly used to interpret climate within ancient sediments on Earth, as well as planetary samples derived from unknown bedrock sources (provenance), depositional environment, and climatic history. However, in this study, comparison of modern sediments produced in end-member climate systems failed to produce patterns that could be correlated with climate on these ternary plots, as samples from different climate regimes largely overlapped. Therefore, we took an alternative approach to investigate multiple weathering signatures all together, using BET surface area, major oxides, heavy metals, trace metals, REEs, mineralogy, and grain size (percentage of clay-sized particles) within the mud fraction using PCAs (Fig. 12). PCAs of our entire data set also produced partially overlapping clusters of temperate glacial (Washington) and tropical (Puerto Rico) data points, whereas other temperate glacial regions (Iceland, Peru, Norway) clustered away from the other groups. These results—combined with provenance considerations inferred from A-CNK-FM and MFW diagrams on bedrock data (Figs. 11A and 12A) and the overlapping Antarctica, Washington, and Puerto Rico data clusters within the PCAs of the mineralogy (Fig. 6) and geochemistry (Fig. 7) of our samples-suggest that subtle differences in provenance significantly affect the "weathering" signatures observed in the sediments collected across our climate end-member field sites, even though we tried to keep the bedrock compositions similar (granitic-granodioritic, with the exception of Iceland).

In a further attempt to separate the climate signature from provenance, we normalized the CIA values of the fluvial sediments to the average bedrock CIA values for each field site (Eq. 3):

$$CIA_n = CIA_{mud}/CIA_{bedrock}$$
. (3)

Then, we compared these normalized ${\rm CIA_n}$ values with the MAT and MAP observed in each field area to investigate if these climate parameters correlated with potential weathering signatures within fluvial settings. However, the correlations between the CIA values and the MAP ($R^2=0.6862$) and MAT ($R^2=0.5239$) were stronger than the correlations observed between bedrock-normalized CIA_n values (R^2 for CIA_n vs. MAP = 0.5538 and R^2 for CIA_n vs. MAT = 0.4226) of the sediments (Fig. 13), suggesting that provenance effects might lead to overestimated CIA-climate correlations.

We then removed the nonglacial (Anza Borrego and Puerto Rico) muds from the data set to investigate the applicability of CIA-climate correlations within only glaciofluvial settings, which diminished correlations between CIA and climate (for both raw and normalized data; Fig. 14). Deng et al. (2022) also reported that CIA values of glaciofluvial muds do not fit traditional trends assumed for CIA-climatic correlations, though CIA and MAT correlated strongly for nonglacial fluvial muds from warmer settings $(R^2 = \sim 0.6)$ in their study. This implies that CIA is not a useful metric for interpreting paleoclimate in glaciofluvial settings, unless weathering trends are being evaluated between proximal and distal regions in a single catchment (i.e., Thorpe et al., 2019), and they should only be used where the composition of the primary source material is well constrained—such as tropical soil/paleosol profiles (i.e., Joo et al., 2018a).

Synthesis and Implications for Paleoclimate Studies

In contrast to many paleoclimate/weathering studies that are limited to tropical settings or data mining from the literature, our study focused on systematically collected sediments from watersheds with similar bedrock compositions (except for Iceland) from various glacial settings with different MAP and MAT, as well as hot-wet and hot-dry nonglacial systems, and various depositional settings to directly test the effects of climate on weathering signatures observed in modern sediments. All samples were collected,

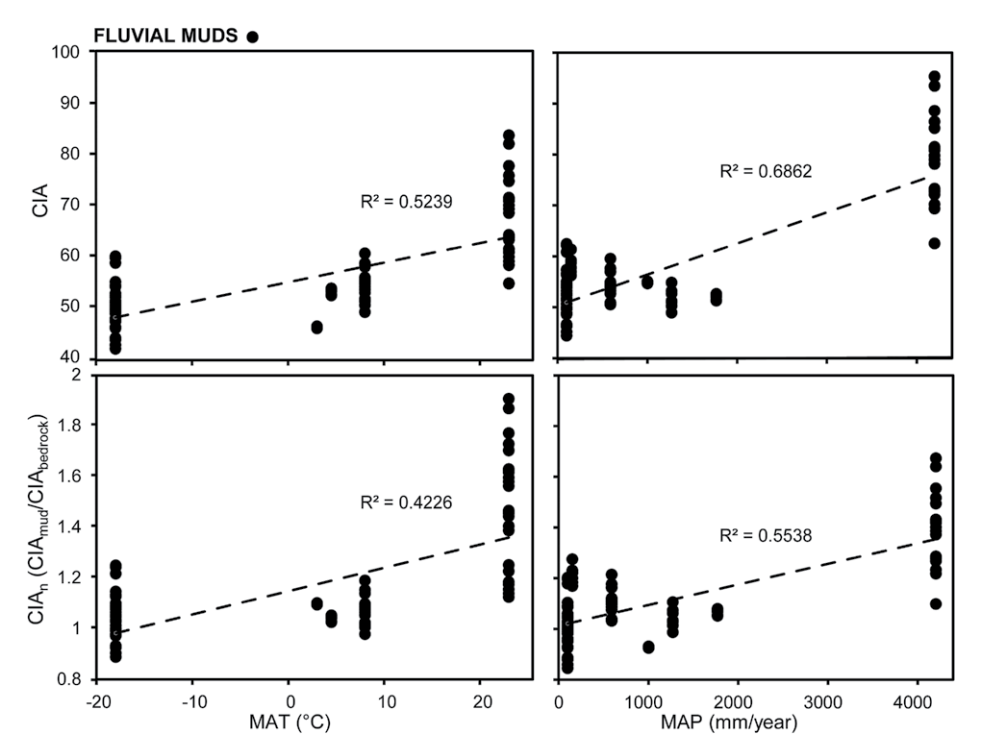


Figure 13. Correlations between chemical index of alteration (CIA) and bedrock-normalized CIA values (CIA $_{\rm n}$) and climatic parameters (mean annual precipitation [MAP] and mean annual temperature [MAT]) based on fluvial samples from all field sites. CIA $_{\rm n}$ corrections reduced the correlation between CIA and climatic parameters, suggesting provenance was leading to overestimated correlations between climate and weathering.

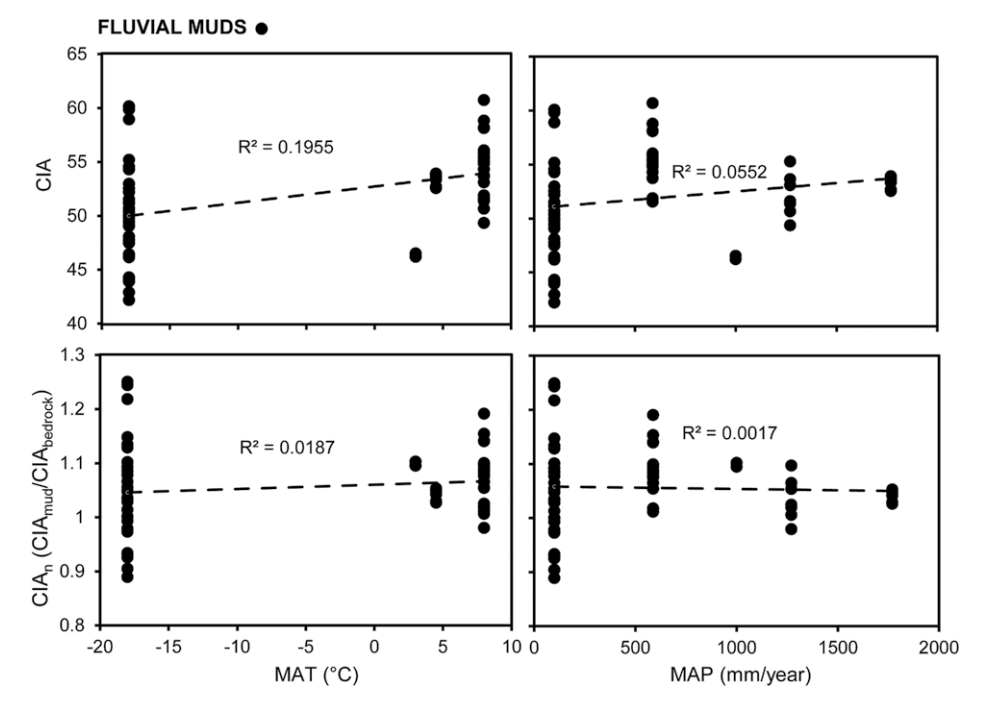


Figure 14. Correlations between chemical index of alteration (CIA) and bedrock-normalized CIA values (CIA $_{\rm n}$) and climatic parameters (mean annual precipitation [MAP] and mean annual temperature [MAT]) based on proglacial fluvial muds. These plots illustrate that there are no significant correlations between CIA and climate parameters within the glacial environments (Puerto Rico and Anza Borrego have been removed).

treated, prepared, and analyzed the same way; therefore, analytical and operator-based variations were minimal. Despite these systematic and careful measures, our study revealed overlapping CIA values and compositional trends on ternary plots (A-CN-K, A-CNK-FM, and MFW), suggesting that differences in provenance outweigh weathering processes, preventing accurate interpretations of climate from fine-grained sediments, especially in sediments derived from intermediate or mixed bedrock. Mafic minerals, as well as other Ca-rich minerals, concentrate within the fine fraction during weathering and transport, resulting in relative enrichment of CaO and correspondingly underestimated CIA values, as also noted in previous studies (i.e., Nesbitt et al., 1996; Siebach et al., 2017; Mangold et al., 2019).

Most of the literature reporting strong correlations between CIA and climate are based on soil profiles or fluvial watersheds in tropical climates (Rasmussen et al., 2011; Yang et al., 2016; Joo et al., 2018a; Mao et al., 2022), which have welldefined chemical weathering trends (increasing Al₂O₃ and clay minerals with weathering, etc.). Our climate (MAP and MAT) and CIA correlation analyses based on sediments from a range of end-member climates in fluvial settings suggest that CIA is not a useful metric for glaciated settings, in agreement with Deng et al. (2022), especially in systems that may incorporate older sediments that have experienced multiple cycles of weathering. Therefore, our results call for caution when applying CIA to interpret climate from fine-grained sediments, especially those derived from glacial, intermediate, or mixedsource environments.

Our results combined with previous studies indicate that CIA and ternary plots may be useful tools for studying weathering in tropical settings with uniform bedrock composition, where elemental (weathering) trends can be directly linked between the bedrock and the derived sediment, such as soil profiles/paleosols. Since provenance often overwhelmed climate signals in our study, even when comparing sites with similar underlying bedrock from very different end-member climate conditions, CIA is not suitable for comparisons between mixed-provenance data sets or where the provenance is unknown. Our observations of overlapping CIA values of glacial muds with CIA values of muds derived from hot climates suggest that relying on CIA can result in erroneous interpretations about weathering and paleoclimate. In addition, CIA values observed in different glacial settings should not be compared directly to determine the relative extent of weathering, but rather could be used within a single setting to determine changes in the extent of weathering over time, if the source rock is known (and is uniform), and the depositional setting remains constant to avoid grain sorting effects. These effects are particularly important to consider in planetary environments, where it may be difficult or impossible to directly link sediments with their source rock(s) (e.g., Mars; Thorpe et al., 2021). Even within closed basins such as impact craters, subtle changes in source rock composition or erosional processes may significantly affect the mineralogy and geochemistry of fine-grained fluvial sediments. For example, subtle changes in sediment transport mechanisms can have significant effects on CIA values, as demonstrated by shifts in CIA values observed after storm-induced mass wasting within a watershed in Puerto Rico (Joo et al., 2018a; Webb et al., 2022).

CONCLUSIONS

Based on the sedimentologic and geochemical data from terrestrial sediments collected across end-member climatic regimes, we conclude that physical, chemical, and biological weathering processes all leave imprints on terrestrial sediments, as inferred from surface area, grain size, geochemistry, and mineralogy combined. However, relatively minor differences in source rock lithology (mineralogy, geochemistry, and texture) overwhelm any climatic signatures that may be present when comparing end-member climate conditions in fine-grained fluvial sediments. In addition, grain size and BET surface area are not significant proxies for climate within a multiprovenance data set of mud-sized sediments from various depositional settings, though they may be valuable for investigating weathering trends within individual field sites.

Weathering indices and ternary plots that are commonly used as proxies to interpret paleoclimate are most useful when applied to well-developed weathering profiles within tropical settings (e.g., Puerto Rico), but they are largely ineffective for identifying climate signals in fine-grained fluvial and glacial sediments formed in other climates. Though CIA values and ternary diagrams (A-CN-K, A-CNK-FM, MFW) have conventionally been used to interpret paleoclimate conditions based on the intensity of weathering, CIA values and position of data within ternary diagrams are heavily affected by the amount of silicate-bound CaO, as higher CaO concentrations result in lower CIA values and pull samples toward the mafic apex of MFW plots. Despite treating our samples to isolate the silicate fraction by removing soluble salts, carbonates, and organic matter, our data set still contained significant variation in CaO content. Even if the weathering intensities of two regions match, higher Ca content (plagioclase, Ca-pyroxene, Ca-rich amphiboles, etc.)

leads to lower CIA values. In addition, CaO is relatively enriched in finer-grained sediments, as mechanically and chemically weaker mafic components rich in Ca are preferentially sorted into the mud fraction, while harder felsic minerals remain within the sand- and gravel-sized grains (i.e., Nesbitt et al., 1996; Mangold et al., 2019). This can cause muds derived from felsic rocks to plot as mafic within ternary plots, hindering interpretations of weathering extent. Therefore, the use of CIA and ternary diagrams for fine-grained terrestrial and planetary sediments, especially sediments derived from intermediate- or mixedcomposition sources, requires caution and additional proxies in order to make realistic climatic interpretations.

Plotting individual major-oxide components from fine-grained sediments on ternary diagrams may intensify small differences in provenance, thus diluting the weathering signatures within the data set and hindering climatic interpretations. Normalizing sediment data based on bedrock composition to reduce the provenance effect reduced correlations with climate parameters (MAP and MAT), suggesting that provenance effects might lead to overestimated CIA-climate correlations. In addition, CIA-climate trends were absent when we excluded sediments formed in hot climates (Anza Borrego and Puerto Rico muds) from the data set.

A synthesis of our overall findings suggests: (1) CIA and ternary plots for weathering are most useful when applied to hot-humid settings with uniform bedrock composition, where elemental (weathering) trends can be traced from the bedrock to first-cycle material (soil profiles/paleosols); (2) CIA values of muds from glacial settings overlap with those from hot and humid climates; and (3) no correlations were observed between climatic parameters (mean annual precipitation and temperature) and CIA in glacial systems, suggesting that CIA is not a useful metric with which to assess paleoclimate in (suspected) glaciated settings.

ACKNOWLEDGMENTS

This project was funded by National Science Foundation (NSF) grants ANT-0842639, EAR-1225162, and EAR-1543344. Project information can be found at the U.S. Antarctic Program Data Center (USAP-DC) website at https://www.usap-dc.org/view/project /p0010181. All data tables associated with this manuscript are available from the USAP-DC at https:// www.usap-dc.org/view/dataset/601599 and as supplemental material at https://doi.org/10.1130/GSAB .S.23900184. We thank Kristen Marra for supplying samples and appreciate her help with sample processing and analyses, as well as her editorial contributions. We thank Claire Curry, Zachary D. Tomlinson, J. Scott Greene, James G. Floyd, and Mark J. Laufersweiler for their valuable comments and suggestions on our data analysis methods.

REFERENCES CITED

- Aitchison, J., 1982, The statistical analysis of compositional data: Journal of the Royal Statistical Society B—Methodological, v. 44, p. 139–160, https://doi.org/10.1111/j.2517-6161.1982.tb01195.x.
- Aitchison, J., and Greenacre, M., 2002, Biplots of compositional data: Journal of the Royal Statistical Society C—Applied Statistics, v. 51, p. 375–392, https://doi.org/10.1111/1467-9876.00275.
- Anderson, S.P., 2005, Glaciers show direct linkage between erosion rate and chemical weathering fluxes: Geomorphology, v. 67, p. 147–157, https://doi.org/10.1016/j.geomorph.2004.07.010.
- Anderson, S.P., Drever, J.I., and Humphrey, N.F., 1997, Chemical weathering in glacial environments: Geology, v. 25, p. 399–402, https://doi.org/10.1130/0091-7613(1997)025<0399:CWIGE>2.3.CO;2.
- Andrews, J.T., and Eberl, D.D., 2007, Quantitative mineralogy of surface sediments on the Iceland shelf, and application to down-core studies of Holocene ice-rafted sediments: Journal of Sedimentary Research, v. 77, p. 469–479, https://doi.org/10.2110/jsr.2007.045.
- Arnalds, O., Dagsson-Waldhauserova, P., and Olafsson, H., 2016, The Icelandic volcanic aeolian environment: Processes and impacts—A review: Aeolian Research, v. 20, p. 176–195, https://doi.org/10.1016/j.aeolia.2016 .01.004.
- Axen, G.J., and Fletcher, J.M., 1998, Late Miocene–Pleistocene extensional faulting, northern Gulf of California, Mexico and Salton Trough, California: International Geology Review, v. 40, p. 217–244, https://doi.org/10.1080/00206819809465207.
- Bahlburg, H., and Dobrzinski, N., 2011, A review of the chemical index of alteration (CIA) and its application to the study of Neoproterozoic glacial deposits and climate transitions, in Arnaud, E., Halverson, G.P., and Shields-Zhou, G., eds., The Geological Record of Neoproterozoic Glaciations: Geological Society, London, Memoir 36, p. 81–92, https://doi.org/10.1144/M36.6.
- Baraer, M., McKenzie, J., Mark, B.G., Gordon, R., Bury, J., Condom, T., Gomez, J., Knox, S., and Fortner, S.K., 2015, Contribution of groundwater to the outflow from ungauged glacierized catchments: A multi-site study in the tropical Cordillera Blanca, Peru: Hydrological Processes, v. 29, p. 2561–2581, https://doi.org/10.1002/hyp.10386.
- Barshad, J., 1966, The effect of a variation of precipitation on the nature of clay mineral formation in soils from acid and basic igneous rocks, *in* Heller, L., and Weiss, A., eds., Proceedings of the International Clay Conference (Jerusalem), Volume 1: Jerusalem, Israel Programme of Scientific Translation, p. 167–173.
- Beck, H.E., Zimmermann, N.E., McVicar, T.R., Vergopolan, N., Berg, A., and Wood, E.F., 2018, Present and future Köppen-Geiger climate classification maps at 1-km resolution: Scientific Data, v. 5, https://doi.org/10.1038 /sdata.2018.214.
- Bedford, C.C., Bridges, J.C., Schwenzer, S.P., Wiens, R.C., Rampe, E.B., Frydenvang, J., and Gasda, P.J., 2019, Alteration trends and geochemical source region characteristics preserved in the fluviolacustrine sedimentary record of Gale crater, Mars: Geochimica et Cosmochimica Acta, v. 246, p. 234–266, https://doi.org/10.1016 /j.gca.2018.11.031.
- Berger, J., et al., 2020, Elemental composition and chemical evolution of geologic materials in Gale crater, Mars: APXS results from Bradbury Landing to the Vera Rubin Ridge: Journal of Geophysical Research: Planets, v. 125, https://doi.org/10.1029/2020JE006536.
- Besette-Kirton, E.K., Cerovski-Darriau, C., Schulz, W.H., Coe, J.A., Kean, J.W., Godt, J.W., Thomas, M.A., and Hughes, S.K., 2019, Landslides triggered by Hurricane Maria: Assessment of an extreme event in Puerto Rico: GSA Today, v. 29, p. 4–10, https://doi.org/10.1130 /GSATG383A.1.
- Bickerton, R.W., and Matthews, J.A., 1993, 'Little Ice Age' variations of outlet glaciers from the Jostedalsbreen ice-cap, southern Norway: A regional lichenometric-dating study of ice-marginal moraine sequences and their climatic significance: Journal of Quaternary Science, v. 8, p. 45–66, https://doi.org/10.1002/jqs.3390080105.

- Biscaye, P.E., 1965, Mineralogy and sedimentation of recent deep-sea clay in the Atlantic Ocean and adjacent seas and oceans: Geological Society of America Bulletin, v. 76, p. 803–832, https://doi.org/10.1130/0016-7606(1965)76[803:MASORD]2.0.CO;2.
- Bish, D.L., and Howard, S.A., 1988, Quantitative phase analysis using the Rietveld method: Journal of Applied Crystallography, v. 21, p. 86–91, https://doi.org/10 .1107/S0021889887009415.
- Bishop, J.L., Fairén, A.G., Michalski, J.R., Gago-Duport, L., Baker, L.L., Velbel, M.A., Gross, C., and Rampe, E.B., 2018, Surface clay formation during short-term warmer and wetter conditions on a largely cold ancient Mars: Nature Astronomy, v. 2, p. 206–213, https://doi.org/10 .1038/s41550-017-0377-9.
- Blott, S.J., Croft, D.J., Pye, K., Saye, S.E., and Wilson, H.E., 2004, Particle size analysis by laser diffraction, in Pye, K., and Croft, D.J., eds., Forensic Geoscience: Principles, Techniques and Applications: Geological Society, London, Special Publication 232, p. 63–73, https://doi .org/10.1144/GSL.SP.2004.232.01.08.
- Bockheim, J.G., and McLeod, M., 2008, Soil distribution in the McMurdo Dry Valleys, Antarctica: Geoderma, v. 144, p. 43–49, https://doi.org/10.1016/j.geoderma .2007.10.015.
- Brown, E.H., and Walker, N.W., 1993, A magma-loading model for Barrovian metamorphism in the south-east Coast Plutonic Complex, British Columbia and Washington: Geological Society of America Bulletin, v. 105, p. 479–500, https://doi.org/10.1130/0016-7606(1993)105<0479:AMLMFB>2.3.CO;2.
- Brunauer, S., Emmett, P.H., and Teller, E., 1938, Adsorption of gases in multimolecular layers: Journal of the American Chemical Society, v. 60, p. 309–319, https://doi.org/10.1021/ja01269a023.
- Bury, J.T., Mark, B.G., McKenzie, J.M., French, A., Baraer, M., Huh, K.I., Zapata Luyo, M.A., and Gómez López, R.J., 2011, Glacier recession and human vulnerability in the Yanamarey watershed of the Cordillera Blanca, Peru: Climatic Change, v. 105, p. 179–206, https://doi.org/10.1007/s10584-010-9870-1.
- Butler, J., Beaumont, C., and Jamieson, R., 2015, Paradigm lost: Buoyancy thwarted by the strength of the Western Gneiss Region (ultra)high-pressure terrane, Norway: Lithosphere, v. 7, p. 379–407, https://doi.org/10.1130
- Campbell, I.B., and Claridge, G.G.C., 2006, Permafrost properties, patterns and processes in the Transantarctic Mountains region: Permafrost and Periglacial Processes, v. 17, p. 215–232, https://doi.org/10.1002/ppp.557.
- Cuozzo, N., Sletten, R.S., Hu, Y., Liu, L., Teng, F.-Z., and Hagedorn, B., 2020, Silicate weathering in Antarctic ice-rich permafrost: Insights using magnesium isotopes: Geochimica et Cosmochimica Acta, v. 278, p. 244–260, https://doi.org/10.1016/j.gca.2019.07.031.
- Daly, C., Neilson, R.P., and Phillips, D.L., 1994, A statistical-topographic model for mapping climatological precipitation over mountainous terrain: Journal of Applied Meteorology and Climatology, v. 33, p. 140–158, https://doi.org/10.1175/1520-0450(1994)033<0140: ASTMFM>2.0.CO;2.
- Daly, C., Halbleib, M., Smith, J.I., Gibson, W.P., Doggett, M.K., Taylor, G.H., Curtis, J., and Pasteris, P.P., 2008, Physiographically sensitive mapping of climatological temperature and precipitation across the conterminous United States: International Journal of Climatology, v. 28, p. 2031–2064, https://doi.org/10.1002/joc.1688.
- Demirel-Floyd, C., 2022, Data and Metadata for Quantifying Surface Area in Muds from the Antarctic Dry Valleys: Implications for Weathering in Glacial Systems: U.S. Antarctic Program (USAP) Data Center Record USAP-1543344_1, https://doi.org/10.15784/601599.
- Demirel-Floyd, C., Soreghan, G.S., and Madden, M.E.E., 2022, Cyanobacterial weathering in warming periglacial sediments: Implications for nutrient cycling and potential biosignatures: Permafrost and Periglacial Processes, v. 33, p. 63–77, https://doi.org/10.1002/ppp .2133.
- Deng, K., Yang, S., and Guo, Y., 2022, A global temperature control of silicate weathering intensity: Nature Communications, v. 13, p. 1781, https://doi.org/10.1038/s41467-022-29415-0.

- Dickinson, W.W., and Rosen, M.R., 2003, Antarctic permafrost: An analogue for water and diagenetic minerals on Mars: Geology, v. 31, p. 199–202, https://doi.org /10.1130/0091-7613(2003)031<0199:APAAFW>2 0 CO:2
- Dogan, A.U., Dogan, M., Onal, M., Sarikaya, Y., Aburub, A., and Wurster, D.E., 2006, Baseline studies of the Clay Minerals Society source clays: Specific surface area by the Brunauer Emmett Teller (BET) method: Clays and Clay Minerals, v. 54, p. 62–66, https://doi.org/10.1346//CCMN.2006.0540108.
- Dogan, M., Dogan, A.U., Yesilyurt, F.I., Alaygut, D., Buckner, I., and Wurster, D.E., 2007, Baseline studies of the Clay Minerals Society special clays: Specific surface area by the Brunauer Emmett Teller (BET) method: Clays and Clay Minerals, v. 55, p. 534–541, https://doi.org/10.1346/CCMN.2007.0550508.
- Doran, P.T., McKay, C.P., Clow, G.D., Dana, G.L., Fountain, A.G., Nylen, T., and Lyons, W.B., 2002, Valley floor climate observations from the McMurdo Dry Valleys, Antarctica, 1986–2000: Journal of Geophysical Research: Atmospheres, v. 107, 4772, https://doi.org/10 .1029/2001JD002045.
- Doran, P.T., McKay, C.P., Fountain, A.G., Nylen, T., McKnight, D.M., Jaros, C., and Barrett, J.E., 2008, Hydrologic response to extreme warm and cold summers in the McMurdo Dry Valleys, East Antarctica: Antarctic Science, v. 20, p. 499–509, https://doi.org/10.1017/S0954102008001272.
- Dorsey, R.J., Housen, B.A., Janecke, S.U., Fanning, C.M., and Spears, A.L.F., 2011, Stratigraphic record of basin development within the San Andreas fault system: Late Cenozoic Fish Creek–Vallecito basin, southern California: Geological Society of America Bulletin, v. 123, p. 771–793, https://doi.org/10.1130/B30168.1.
- Eberl, D.D., 2003, User Guide to RockJock—A Program for Determining Quantitative Mineralogy from X-Ray Diffraction Data: U.S. Geological Survey Open-File Report 2003-78, 47 p., https://doi.org/10.3133/ofr200378.
- Egli, M., Fitze, P., and Mirabella, A., 2001, Weathering and evolution of soils formed on granitic, glacial deposits: Results from chronosequences of Swiss alpine environments: Catena, v. 45, p. 19–47, https://doi.org/10.1016 /S0341-8162(01)00138-2.
- Ehlmann, B., et al., 2011, Subsurface water and clay mineral formation during the early history of Mars: Nature, v. 479, p. 53–60, https://doi.org/10.1038/nature10582.
- Erikson, E.H., 1977, Petrology and petrogenesis of the Mount Stuart batholith—Plutonic equivalent of the high-alumina basalt association?: Contributions to Mineralogy and Petrology, v. 60, p. 183–207, https:// doi.org/10.1007/BF00372281.
- Fedo, C.M., Wayne Nesbitt, H., and Young, G.M., 1995, Unraveling the effects of potassium metasomatism in sedimentary rocks and paleosols, with implications for paleoweathering conditions and provenance: Geology, v. 23, p. 921–924, https://doi.org/10.1130/0091-7613(1995)023<0921:UTEOPM>2.3.CO;2.
- Filzmoser, P., Hron, K., and Reimann, C., 2009, Principal component analysis for compositional data with outliers: Environmetrics, v. 20, p. 621–632, https://doi.org /10.1002/env.966.
- Fletcher, R.C., Buss, H.L., and Brantley, S.L., 2006, A spheroidal weathering model coupling porewater chemistry to soil thicknesses during steady-state denudation: Earth and Planetary Science Letters, v. 244, p. 444–457, https://doi.org/10.1016/j.epsl.2006.01.055.
- Fountain, A.G., et al., 1999, Physical controls on the Taylor Valley ecosystem, Antarctica: Bioscience, v. 49, p. 961– 971, https://doi.org/10.1525/bisi.1999.49.12.961.
- Girty, G.H., Colby, T.A., Rayburn, J.Z., Parizek, J.R., and Voyles, E.M., 2013, Biotite-controlled linear compositional weathering trends in tonalitic to quartz dioritic saprock, Santa Margarita Ecological Reserve, southern California, USA: Catena, v. 105, p. 40–51, https://doi .org/10.1016/j.catena.2013.01.001.
- Goldberg, K., and Humayun, M., 2010, The applicability of the chemical index of alteration as a paleoclimatic indicator: An example from the Permian of the Paraná Basin, Brazil: Palaeogeography, Palaeoclimatology, Palaeoecology, v. 293, p. 175–183, https://doi.org/10.1016 /j.palaeo.2010.05.015.

- Goldich, S.S., 1938, A study in rock-weathering: The Journal of Geology, v. 46, p. 17–58, https://doi.org/10.1086/624619
- Gooseff, M.N., McKnight, D.M., Lyons, W.B., and Blum, A.E., 2002, Weathering reactions and hyporheic exchange controls on stream water chemistry in a glacial meltwater stream in the McMurdo Dry Valleys: Water Resources Research, v. 38, p. 15-1–15-17, https://doi .org/10.1029/2001WR000834.
- Gordon, R.P., Lautz, L.K., McKenzie, J.M., Mark, B.G., Chavez, D., and Baraer, M., 2015, Sources and pathways of stream generation in tropical proglacial valleys of the Cordillera Blanca, Peru: Journal of Hydrology (Amsterdam), v. 522, p. 628–644, https://doi.org/10 .1016/j.jhydrol.2015.01.013.
- Gordon, S.M., Whitney, D.L., Teyssier, C., and Fossen, H., 2013, U-Pb dates and trace-element geochemistry of zircon from migmatite, Western Gneiss Region, Norway: Significance for history of partial melting in continental subduction: Lithos, v. 170–171, p. 35–53, https:// doi.org/10.1016/j.lithos.2013.02.003.
- Grunsky, E.C., Mueller, U.A., and Corrigan, D., 2014, A study of the lake sediment geochemistry of the Melville Peninsula using multivariate methods: Applications for predictive geological mapping: Journal of Geochemical Exploration, v. 141, p. 15–41, https://doi.org/10.1016/j .gexplo.2013.07.013.
- Guglielmin, M., Cannone, N., Strini, A., and Lewkowicz, A.G., 2005, Biotic and abiotic processes on granite weathering landforms in a cryotic environment, Northern Victoria Land, Antarctica: Permafrost and Periglacial Processes, v. 16, p. 69–85, https://doi.org/10.1002/ppp.514.
- Hall, B.L., and Denton, G.H., 2005, Surficial geology and geomorphology of eastern and central Wright Valley, Antarctica: Geomorphology, v. 64, p. 25–65, https://doi. org/10.1016/j.geomorph.2004.05.002.
- Hall, B.L., Denton, G.H., Lux, D.R., and Bockheim, J.G., 1993, Late Tertiary Antarctic paleoclimate and icesheet dynamics inferred from surficial deposits in Wright Valley: Geografiska Annaler A—Physical Geography, v. 75, p. 239–267, https://doi.org/10.1080 /04353676.1993.11880396.
- Hall, B.L., Denton, G.H., and Hendy, C.H., 2000, Evidence from Taylor Valley for a grounded ice sheet in the Ross Sea, Antarctica: Geografiska Annaler A—Physical Geography, v. 82, p. 275–303, https://doi.org/10.1111 /j.0435-3676.2000.00126.x.
- Harnois, L., 1988, The CIW index: A new chemical index of weathering: Sedimentary Geology, v. 55, p. 319–322, https://doi.org/10.1016/0037-0738(88)90137-6.
- Higgins, S.M., Hendy, C.H., and Denton, G.H., 2000, Geochronology of Bonney Drift, Taylor Valley, Antarctica: Evidence for interglacial expansions of Taylor Glacier: Geografiska Annaler A—Physical Geography, v. 82, p. 391–409, https://doi.org/10.1111/j.0435-3676.2000 .00130.x.
- Horowitz, A.J., and Elrick, K.A., 1987, The relation of stream sediment surface area, grain size and composition to trace element chemistry: Applied Geochemistry, v. 2, p. 437–451, https://doi.org/10.1016 /0883-2927(87)90027-8.
- Hron, K., Templ, M., and Filzmoser, P., 2010, Imputation of missing values for compositional data using classical and robust methods: Computational Statistics & Data Analysis, v. 54, p. 3095–3107, https://doi.org/10.1016 /j.csda.2009.11.023.
- Huang, X., Jiang, H., Li, Y., Ma, Y., Tang, H., Ran, W., and Shen, Q., 2016, The role of poorly crystalline iron oxides in the stability of soil aggregate–associated organic carbon in a rice-wheat cropping system: Geoderma, v. 279, p. 1–10, https://doi.org/10.1016/j.geoderma 2016.05.011
- Hurowitz, J.A., et al., 2017, Redox stratification of an ancient lake in Gale crater, Mars: Science, v. 356, https://doi. org/10.1126/science.aah6849.
- Jacobson, A.D., Grace Andrews, M., Lehn, G.O., and Holmden, C., 2015, Silicate versus carbonate weathering in Iceland: New insights from Ca isotopes: Earth and Planetary Science Letters, v. 416, p. 132–142, https:// doi.org/10.1016/j.epsl.2015.01.030.
- Joo, Y.J., Elwood Madden, M.E., and Soreghan, G.S., 2016, Chemical and physical weathering in a hot-arid,

- tectonically active alluvial system of Anza Borrego Desert, California: Sedimentology, v. 63, p. 1065–1083, https://doi.org/10.1111/sed.12249.
- Joo, Y.J., Elwood Madden, M.E., and Soreghan, G.S., 2018a, Anomalously low chemical weathering in fluvial sediment of a tropical watershed (Puerto Rico): Geology, v. 46, p. 691–694, https://doi.org/10.1130/G40315.1.
- Joo, Y.J., Soreghan, A.M., Madden, M.E.E., and Soreghan, G.S., 2018b, Quantification of particle shape by an automated image analysis system: A case study in natural sediment samples from extreme climates: Geosciences Journal, v. 22, p. 525–532, https://doi.org/10.1007 /s12303-018-0025-0.
- Joo, Y.J., Sim, M.S., Elwood Madden, M.E., and Soreghan, G.S., 2022, Significance of the terrestrial sink in the biogeochemical sulfur cycle: Geophysical Research Letters, v. 49, https://doi.org/10.1029/2021GL097009.
- Kaser, G., Ames, A., and Zamora, M., 1990, Glacier fluctuations and climate in the Cordillera Blanca, Peru: Annals of Glaciology, v. 14, p. 136–140, https://doi.org/10 .3189/S0260305500008430.
- Kaser, G., Juen, I., Georges, C., Gómez, J., and Tamayo, W., 2003, The impact of glaciers on the runoff and the reconstruction of mass balance history from hydrological data in the tropical Cordillera Blanca, Perú: Journal of Hydrology (Amsterdam), v. 282, p. 130–144, https://doi .org/10.1016/S0022-1694(03)00259-2.
- Kelly, L.C., Cockell, C.S., Thorsteinsson, T., Marteinsson, V., and Stevenson, J., 2014. Pioneer microbial communities of the Fimmvörðuháls lava flow, Eyjafjallajökull, Iceland: Microbial Ecology, v. 68, p. 504–518, https:// doi.org/10.1007/s00248-014-0432-3.
- Kottek, M., Grieser, J., Beck, C., Rudolf, B., and Rubel, F., 2006, World Map of the Köppen-Geiger climate classification updated: Meteorologische Zeitschrift (Berlin), v. 15, p. 259–263, https://doi.org/10.1127/0941-2948 /2006/0130.
- Lepore, C., Kamal, S.A., Shanahan, P., and Bras, R.L., 2012, Rainfall-induced landslide susceptibility zonation of Puerto Rico: Environmental Earth Sciences, v. 66, p. 1667–1681, https://doi.org/10.1007/s12665-011 -0976-1.
- Levy, J.S., Head, J.W., and Marchant, D.R., 2008, The role of thermal contraction crack polygons in cold-desert fluvial systems: Antarctic Science, v. 20, p. 565–579, https://doi.org/10.1017/S0954102008001375.
- Levy, J.S., Fountain, A.G., Gooseff, M.N., Welch, K.A., and Lyons, W.B., 2011, Water tracks and permafrost in Taylor Valley, Antarctica: Extensive and shallow groundwater connectivity in a cold desert ecosystem: Geological Society of America Bulletin, v. 123, p. 2295–2311, https://doi.org/10.1130/B30436.1.
- Levy, J.S., Fountain, A.G., Gooseff, M.N., Barrett, J.E., Vantreese, R., Welch, K.A., Lyons, W.B., Nielsen, U.N., and Wall, D.H., 2014, Water track modification of soil ecosystems in the Lake Hoare basin, Taylor Valley, Antarctica: Antarctic Science, v. 26, p. 153–162, https://doi .org/10.1017/S095410201300045X.
- Lewis, S., and Birnie, J., 2001, Little Ice Age alluvial fan development in Langedalen, western Norway: Geografiska Annaler A—Physical Geography, v. 83, p. 179–190, https://doi.org/10.1111/1468-0459.00153.
- Li, C., and Yang, S., 2010, Is chemical index of alteration (CIA) a reliable proxy for chemical weathering in global drainage basins?: American Journal of Science, v. 310, p. 111–127, https://doi.org/10.2475/02.2010.03.
- Love, D.A., Clark, A.H., and Glover, J.K., 2004, The lithologic, stratigraphic, and structural setting of the giant Antamina copper-zinc skarn deposit, Ancash, Peru: Economic Geology, v. 99, p. 887–916, https://doi.org/10.2113/econgeo.99.5.887.
- Lyons, W.B., Dailey, K.R., Welch, K.A., Deuerling, K.M., Welch, S.A., and McKnight, D.M., 2015, Antarctic streams as a potential source of iron for the Southern Ocean: Geology, v. 43, p. 1003–1006, https://doi.org/10.1130/G36989.1.
- Mangold, N., et al., 2019, Chemical alteration of fine-grained sedimentary rocks at Gale crater: Icarus, v. 321, p. 619–631, https://doi.org/10.1016/j.icarus.2018.11.004.
- Mann, P., Hippolyte, J.-C., Grindlay, N.R., and Abrams, L.J., 2005, Neotectonics of southern Puerto Rico and its offshore margin, in Mann, P., ed., Active Tectonics and

- Seismic Hazards of Puerto Rico, the Virgin Islands, and Offshore Areas: Geological Society of America Special Paper 385, p. 173–214, https://doi.org/10.1130/0-8137-2385-X.173.
- Mao, H.-R., Cui, L.-F., Zhang, Z.-J., Xu, S., Liu, C.-Q., and Zhao, Z.-Q., 2022, Influence of monsoon climate on chemical weathering of granitic regoliths: Global Biogeochemical Cycles, v. 36, https://doi.org/10.1029/ /2022GB007362.
- Marra, K.R., Soreghan, G.S., Elwood Madden, M.E., Keiser, L.J., and Hall, B.L., 2014, Trends in grain size and BET surface area in cold-arid versus warm-semiarid fluvial systems: Geomorphology, v. 206, p. 483–491, https:// doi.org/10.1016/j.geomorph.2013.10.018.
- Marra, K.R., Madden, M.E.E., Soreghan, G.S., and Hall, B.L., 2015, BET surface area distributions in polar stream sediments: Implications for silicate weathering in a cold-arid environment: Applied Geochemistry, v. 52, p. 31–42, https://doi.org/10.1016/j.apgeochem .2014.11.005.
- Marra, K.R., Madden, M.E.E., Soreghan, G.S., and Hall, B.L., 2017, Chemical weathering trends in fine-grained ephemeral stream sediments of the McMurdo Dry Valleys, Antarctica: Geomorphology, v. 281, p. 13–30, https://doi.org/10.1016/j.geomorph.2016.12.016.
- Martín-Fernández, J.A., Barceló-Vidal, C., and Pawlowsky-Glahn, V., 2003, Dealing with zeros and missing values in compositional data sets using nonparametric imputation: Mathematical Geology, v. 35, p. 253–278, https://doi.org/10.1023/A:1023866030544.
- Martín-Fernández, J.A., Hron, K., Templ, M., Filzmoser, P., and Palarea-Albaladejo, J., 2012, Model-based replacement of rounded zeros in compositional data: Classical and robust approaches: Computational Statistics & Data Analysis, v. 56, p. 2688–2704, https://doi.org/10 .1016/j.csda.2012.02.012.
- Maurice, P.A., McKnight, D.M., Leff, L., Fulghum, J.E., and Gooseff, M., 2002, Direct observations of aluminosilicate weathering in the hyporheic zone of an Antarctic Dry Valley stream: Geochimica et Cosmochimica Acta, v. 66, p. 1335–1347, https://doi.org/10.1016/S0016 -7037(01)00890-0.
- McLennan, S.M., et al., 2014, Elemental geochemistry of sedimentary rocks at Yellowknife Bay, Gale crater, Mars: Science, v. 343, https://doi.org/10.1126/science.1244734.
- Monroe, W.H., 1980, Geology of the Middle Tertiary Formations of Puerto Rico: U.S. Geological Survey Professional Paper 953, 93 p., https://doi.org/10.3133/pp953.
- Murphy, S.F., Stallard, R.F., Larsen, M.C., and Gould, W.A., 2012, Physiography, Geology, and Land Cover of Four Watersheds in Eastern Puerto Rico: U.S. Geological Survey Professional Paper 1789-A, 24 p., http://www.fs .usda.gov/treesearch/pubs/41669 (accessed July 2022).
- Nesbitt, H.W., and Young, G.M., 1982, Early Proterozoic climates and plate motions inferred from major element chemistry of lutites: Nature, v. 299, p. 715–717, https://doi.org/10.1038/299715a0.
- Nesbitt, H.W., and Young, G.M., 1989, Formation and diagenesis of weathering profiles: The Journal of Geology, v. 97, p. 129–147, https://doi.org/10.1086/629290.
- Nesbitt, H.W., Young, G.M., McLennan, S.M., and Keays, R.R., 1996, Effects of chemical weathering and sorting on the petrogenesis of siliciclastic sediments, with implications for provenance studies: The Journal of Geology, v. 104, p. 525–542, https://doi.org/10.1086 /629850.
- Nesbitt, H.W., Fedo, C.M., and Young, G.M., 1997, Quartz and feldspar stability, steady and non-steady-state weathering, and petrogenesis of siliciclastic sands and muds: The Journal of Geology, v. 105, p. 173–192, https://doi.org/10.1086/515908.
- Nezat, C.A., Lyons, W.B., and Welch, K.A., 2001, Chemical weathering in streams of a polar desert (Taylor Valley, Antarctica): Geological Society of America Bulletin, v. 113, p. 1404–1408, https://doi.org/10.1130/0016-7606(2001)113
- Nguyen, M.L., Goldfarb, J.L., Plante, A.F., Lau, B.L.T., and Hockaday, W.C., 2019, Sorption temperature and the stability of iron-bound soil organic matter: Geoderma, v. 341, p. 93–99, https://doi.org/10.1016/j.geoderma .2019.01.040.

- Ohta, T., and Arai, H., 2007, Statistical empirical index of chemical weathering in igneous rocks: A new tool for evaluating the degree of weathering: Chemical Geology, v. 240, p. 280–297, https://doi.org/10.1016/j.chemgeo.2007.02.017.
- Ólafsson, H., Furger, M., and Brümmer, B., 2007, The weather and climate of Iceland: Meteorologische Zeitschrift (Berlin), v. 16, p. 5–8, https://doi.org/10.1127/0941-2948/2007/0185.
- Palarea-Albaladejo, J., Martín-Fernández, J.A., and Buccianti, A., 2014, Compositional methods for estimating elemental concentrations below the limit of detection in practice using R: Journal of Geochemical Exploration, v. 141, p. 71–77, https://doi.org/10.1016/j.gexplo.2013.09.003.
- Parker, A., 1970, An index of weathering for silicate rocks: Geological Magazine, v. 107, p. 501–504, https://doi.org/10.1017/S0016756800058581.
- Peretyazhko, T.S., Sutter, B., Morris, R.V., Agresti, D.G., Le, L., and Ming, D.W., 2016, Fe/Mg smectite formation under acidic conditions on early Mars: Geochimica et Cosmochimica Acta, v. 173, p. 37–49, https://doi.org /10.1016/j.gca.2015.10.012.
- Prospero, J.M., Bullard, J.E., and Hodgkins, R., 2012, High-latitude dust over the North Atlantic: Inputs from Icelandic proglacial dust storms: Science, v. 335, p. 1078–1082, https://doi.org/10.1126/science 1217447.
- Rasmussen, C., Brantley, S., Richter, D.D., Blum, A., Dixon, J., and White, A.F., 2011, Strong climate and tectonic control on plagioclase weathering in granitic terrain: Earth and Planetary Science Letters, v. 301, p. 521–530, https://doi.org/10.1016/j.epsl.2010.11.037.
- Reiners, P.W., Ehlers, T.A., Mitchell, S.G., and Montgomery, D.R., 2003, Coupled spatial variations in precipitation and long-term erosion rates across the Washington Cascades: Nature, v. 426, p. 645–647, https://doi.org/10.1038/nature02111.
- Remeika, P., and Lindsay, L., 1992, Geology of Anza-Borrego: Edge of Creation: San Diego, California, Sunbelt Publications, 218 p., https://sunbeltpublications.com/shop/geology-of-anza-borrego/.
- Ren, X., Nie, J., Saylor, J.E., Li, H., Bush, M.A., and Horton, B.K., 2019, Provenance control on chemical weathering index of fluvio-lacustrine sediments: Evidence from the Qaidam Basin, NE Tibetan Plateau: Geochemistry, Geophysics, Geosystems, v. 20, p. 3216–3224, https:// doi.org/10.1029/2019GC008330.
- Robert, C., and Kennett, J.P., 1992, Paleocene and Eocene kaolinite distribution in the South Atlantic and Southern Ocean: Antarctic climatic and paleoceanographic implications: Marine Geology, v. 103, p. 99–110, https://doi .org/10.1016/0025-3227(92)90010-F.
- Robert, C., and Kennett, J.P., 1994, Antarctic subtropical humid episode at the Paleocene-Eocene boundary: Claymineral evidence: Geology, v. 22, p. 211–214, https://doi.org/10.1130/0091-7613(1994)022<0211:ASHE AT>2.3.CO;2.
- Robert, C., and Kennett, J.P., 1997, Antarctic continental weathering changes during Eocene—Oligocene cryosphere expansion: Clay mineral and oxygen isotope evidence: Geology, v. 25, p. 587–590, https://doi.org/10.1130/0091-7613(1997)025<0587:ACWCDE>2.3.CO;2.
- Rogers, C.S., Cram, C.M., Pease, M.H., Jr.,, and Tischler, M.S., 1979, Geologic Map of the Yabucoa and Punta Tuna Quadrangles, Puerto Rico: U.S. Geological Survey IMAP 1086, scale 1:20,000, https://doi.org/10.3133 /i1086.
- Root, D.B., Hacker, B.R., Gans, P.B., Ducea, M.N., Eide, E.A., and Mosenfelder, J.L., 2005, Discrete ultrahighpressure domains in the Western Gneiss Region, Norway: Implications for formation and exhumation: Journal of Metamorphic Geology, v. 23, p. 45–61, https://doi.org/10.1111/j.1525-1314.2005.00561.x.
- Rye, N., Nesje, A., Lien, R., Blikra, L.H., Eiken, O., Hole, P.A., and Torsnes, I., 1997, Glacial geology and deglaciation chronology of the area between inner Nordfjord and Jostedalsbreen Strynefjellet, western Norway: Norwegian Journal of Geology (Norsk Geologisk Tidsskrift), v. 77, p. 13.
- Siame, L.L., Sébrier, M., Bellier, O., and Bourles, D., 2006, Can cosmic ray exposure dating reveal the normal

- faulting activity of the Cordillera Blanca fault, Peru?: Revista de la Asociación Geológica Argentina, v. 61, p. 536–544.
- Siebach, K.L., Baker, M.B., Grotzinger, J.P., McLennan, S.M., Gellert, R., Thompson, L.M., and Hurowitz, J.A., 2017, Sorting out compositional trends in sedimentary rocks of the Bradbury group (Aeolis Palus), Gale crater, Mars: Journal of Geophysical Research: Planets, v. 122, p. 295–328, https://doi.org/10.1002/2016JE005195.
- Sigmundsson, F., et al., 2010, Intrusion triggering of the 2010 Eyjafjallajökull explosive eruption: Nature, v. 468, p. 426–430, https://doi.org/10.1038/nature09558.
- Smith, G.O., 1903, Description of the Mount Stuart Quadrangle: U.S. Geological Survey, 10 p., https://pubs.usgs.gov/gf/106/text.pdf.
- Soreghan, G.S., Joo, Y.J., Elwood Madden, M.E., and Van Deventer, S.C., 2016, Silt production as a function of climate and lithology under simulated comminution: Quaternary International, v. 399, p. 218–227, https:// doi.org/10.1016/j.quaint.2015.05.010.
- Soreghan, M.J., and Soreghan, G.S., 2007, Whole-rock geochemistry of Upper Paleozoic loessite, western Pangaea: Implications for paleo-atmospheric circulation: Earth and Planetary Science Letters, v. 255, p. 117–132, https://doi.org/10.1016/j.epsl.2006.12.010.
- Stumpf, A.R., Elwood Madden, M.E., Soreghan, G.S., Hall, B.L., Keiser, L.J., and Marra, K.R., 2012, Glacier meltwater stream chemistry in Wright and Taylor Valleys, Antarctica: Significant roles of drift, dust and biological processes in chemical weathering in a polar climate: Chemical Geology, v. 322–323, p. 79–90, https://doi. org/10.1016/j.chemgeo.2012.06.009.
- Thiry, M., 2000, Palaeoclimatic interpretation of clay minerals in marine deposits: An outlook from the continental origin: Earth-Science Reviews, v. 49, p. 201–221, https://doi.org/10.1016/S0012-8252(99)00054-9.
- Thorpe, M.T., Hurowitz, J.A., and Dehouck, E., 2019, Sediment geochemistry and mineralogy from a glacial terrain river system in southwest Iceland: Geochimica et Cosmochimica Acta, v. 263, p. 140–166, https://doi.org/10.1016/j.gca.2019.08.003.
- Thorpe, M.T., Hurowitz, J.A., and Siebach, K.L., 2021, Source-to-sink terrestrial analogs for the paleoenvironment of Gale crater, Mars: Journal of Geophysical Research: Planets, v. 126, https://doi.org/10.1029 /2020JE006530.
- Ugolini, F.C., 1967, Soils of Mount Erebus, Antarctica: New Zealand Journal of Geology and Geophysics, v. 10, p. 431–442, https://doi.org/10.1080/00288306.1967 .10426747.
- van den Boogaart, K.G., and Tolosana-Delgado, R., 2008, "compositions": A unified R package to analyze compo-

- sitional data: Computers & Geosciences, v. 34, p. 320–338, https://doi.org/10.1016/j.cageo.2006.11.017.
- Velbel, M.A., 1993, Temperature dependence of silicate weathering in nature: How strong a negative feedback on long-term accumulation of atmospheric CO₂ and global greenhouse warming?: Geology, v. 21, p. 1059–1062, https://doi.org/10.1130/0091-7613(1993)021<-1059;TDOSWI>-2.3.CO:2.
- von Eynatten, H., Tolosana-Delgado, R., and Karius, V., 2012, Sediment generation in modern glacial settings: Grain-size and source-rock control on sediment composition: Sedimentary Geology, v. 280, p. 80–92, https:// doi.org/10.1016/j.sedgeo.2012.03.008.
- Vuille, M., Francou, B., Wagnon, P., Juen, I., Kaser, G., Mark, B.G., and Bradley, R.S., 2008, Climate change and tropical Andean glaciers: Past, present and future: Earth-Science Reviews, v. 89, p. 79–96, https://doi.org/10.1016/j.earscirev.2008.04.002.
- Wang, P., Du, Y., Yu, W., Algeo, T.J., Zhou, Q., Xu, Y., Qi, L., Yuan, L., and Pan, W., 2020, The chemical index of alteration (CIA) as a proxy for climate change during glacial-interglacial transitions in Earth history: Earth-Science Reviews, v. 201, https://doi.org/10.1016/j .earscirev.2019.103032.
- Webb, N., Regmi, N., Soreghan, G., Madden, A., Sylvester, J., Colon, F., Demirel-Floyd, C., and Elwood Madden, M., 2022, Effects of mass wasting on the physiochemical properties of fluvial sediments in Puerto Rico following Hurricane Maria: Journal of Geophysical Research: Earth Surface, v. 127, https://doi.org/10.1029 /2021JF006509.
- Weidong, L., Baret, F., Xingfa, G., Qingxi, T., Lanfen, Z., and Bing, Z., 2002, Relating soil surface moisture to reflectance: Remote Sensing of Environment, v. 81, p. 238– 246, https://doi.org/10.1016/S0034-4257(01)00347-9.
- White, A.F., and Blum, A.E., 1995, Effects of climate on chemical weathering in watersheds: Geochimica et Cosmochimica Acta, v. 59, p. 1729–1747, https://doi.org/10.1016/0016-7037(95)00078-E.
- White, A.F., and Brantley, S.L., 2003, The effect of time on the weathering of silicate minerals: Why do weathering rates differ in the laboratory and field?: Chemical Geology, v. 202, p. 479–506, https://doi.org/10.1016/j .chemgeo.2003.03.001.
- White, A.F., and Buss, H.L., 2014, Natural weathering rates of silicate minerals, in Holland, H.D., and Turekian, K.K., eds., Treatise on Geochemistry (second edition): Amsterdam, Netherlands, Elsevier, p. 115–155, https:// doi.org/10.1016/B978-0-08-095975-7.00504-0.
- White, A.F., and Peterson, M.L., 1990, Role of reactivesurface-area characterization in geochemical kinetic models, in Melchior, D.C., and Bassett, R.L., eds.,

- Chemical Modeling of Aqueous Systems II: American Chemical Society (ACS) Symposium Series 416, p. 461–475, https://doi.org/10.1021/bk-1990-0416.ch035.
- White, A.F., Blum, A.E., Schulz, M.S., Bullen, T.D., Harden, J.W., and Peterson, M.L., 1996, Chemical weathering rates of a soil chronosequence on granitic alluvium: I. Quantification of mineralogical and surface area changes and calculation of primary silicate reaction rates: Geochimica et Cosmochimica Acta, v. 60, p. 2533–2550, https://doi.org/10.1016/0016-7037(96)00106-8.
- White, A.F., Blum, A.E., Schulz, M.S., Vivit, D.V., Stonestrom, D.A., Larsen, M., Murphy, S.F., and Eberl, D., 1998, Chemical weathering in a tropical watershed, Luquillo Mountains, Puerto Rico: I. Long-term versus short-term weathering fluxes: Geochimica et Cosmochimica Acta, v. 62, p. 209–226, https://doi.org/10.1016/S0016-7037(97)00335-9.
- White, A.F., Blum, A.E., Bullen, T.D., Vivit, D.V., Schulz, M., and Fitzpatrick, J., 1999, The effect of temperature on experimental and natural chemical weathering rates of granitoid rocks: Geochimica et Cosmochimica Acta, v. 63, p. 3277–3291, https://doi.org/10.1016/S0016-7037(99)00250-1.
- Wilson, J.J., Reyes Rivera, L., and Garayar, S., J., 1995, Geología de los Cuadrángulos de Pallasca, Tayabamba, Corongo, Pomabamba, Carhuaz y Huari. Hojas: 17-h, 17-i,18-h, 18-i, 19-h, y 19-i: Instituto Geológico, Minero y Metalúrgico (INGEMMET [Peru]) Boletín A 60, https://repositorio.ingemmet.gob.pe/handle /20.500.12544/182 (accessed July 2022).
- Wise, W.S., 2005, MINERALS | Zeolites, in Selley, R.C., Cocks, L.R.M., and Plimer, I.R., eds., Encyclopedia of Geology: San Diego, California, Academic Press, p. 591–600, https://doi.org/10.1016/B0-12-369396-9 /00270-7.
- Xiao, S., Liu, W., Li, A., Yang, S., and Lai, Z., 2010, Pervasive autocorrelation of the chemical index of alteration in sedimentary profiles and its palaeoenvironmental implications: Sedimentology, v. 57, p. 670–676, https://doi.org/10.1111/j.1365-3091.2009.01113.x.
- Yang, J., Cawood, P.A., Du, Y., Li, W., and Yan, J., 2016, Reconstructing early Permian tropical climates from chemical weathering indices: Geological Society of America Bulletin, v. 128, p. 739–751, https://doi.org/10.1130/B31371.1.

SCIENCE EDITOR: MIHAI DUCEA ASSOCIATE EDITOR: TROY RASBURY

MANUSCRIPT RECEIVED 5 DECEMBER 2022 REVISED MANUSCRIPT RECEIVED 13 MAY 2023 MANUSCRIPT ACCEPTED 7 AUGUST 2023